Electronic Supplementary Information

Construction of Pd-based coordination cages with three geometrically distinct ligands

Ru-Jin Li, Jean de Montmollin, Farzaneh Fadaei-Tirani, Rosario Scopelliti, and Kay Severin*

Institut of Chemical Sciences and Engineering, École Polytechnique Fédérale de Lausanne (EPFL), 1015 Lausanne, Switzerland

Table of contents

1. General

All chemicals were obtained from commercial sources and used without further purification unless stated otherwise. The ligands **L1**,[S1] **L1'**,[S2] **L2**,[S3] **L2'**,[S4] **L3**,[S5] and **L3'**[S6] (Figure S1) were prepared according to (or in analogy to) procedures described in the literature.

NMR spectra were measured on a Bruker Avance III HD spectrometer (^{1}H: 400 MHz) equipped with a BBFO-Plus$_z$ 5 mm probe, a Bruker Avance III spectrometer (^{1}H: 400 MHz) equipped with a BBFO$_z$ 5 mm probe. The chemical shifts are reported in parts per million (ppm) using the solvent residual signal as a reference.

High resolution mass spectrometry experiments were carried out using a hybrid ion trap-Orbitrap Fourier transform mass spectrometer, Orbitrap Elite (Thermo Scientific) equipped with a TriVersa Nanomate (Advion) nano-electrospray ionization source.

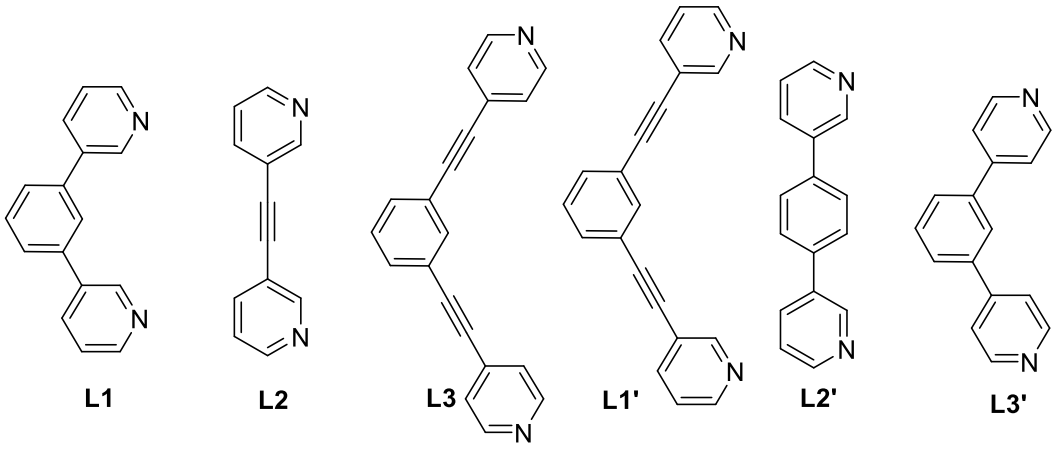

Figure S1. Structures of the ligands **L1**–**L3** and **L1'**–**L3'**.

2. Syntheses

2.1. Synthesis of $[Pd_4(\mathbf{L2})_8](BF_4)_8$

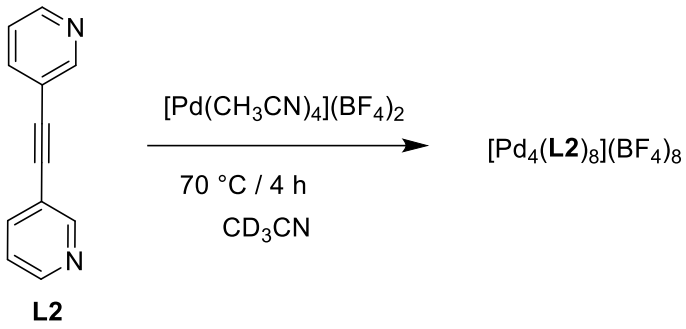

The cage $[Pd_4(\mathbf{L2})_8](BF_4)_8$ was synthesized by stirring a mixture of ligand **L2** (9 µmol, 200 µL of a 45 mM stock solution of **L2** in CD_3CN) and $[Pd(CH_3CN)_4](BF_4)_2$ (4.5 µmol, 150 µL of a 30 mM stock solution in CD_3CN) in 650 µL CD_3CN at 70 °C for 4 h to give 1000 µL of a 1.13 mM solution of cage $[Pd_4(\mathbf{L2})_8](BF_4)_8$. ^{1}H NMR (400 MHz, CD_3CN) δ 9.73 (d, *J* = 1.8 Hz, 1H), 9.26 (dd, *J* = 5.9, 1.4 Hz, 1H), 8.97 (d, *J* = 1.8 Hz, 1H), 8.91 (dd, *J* = 5.8, 1.4 Hz, 1H), 8.20 (dt, *J* = 8.2, 1.5 Hz, 1H), 8.01 (dt, *J* = 8.2, 1.5 Hz, 1H), 7.76 (ddd, *J* = 8.1, 5.9, 0.8 Hz, 1H), 7.55 (dd, *J* = 8.1, 5.8 Hz, 1H) (for an assignment of the signals, see Figure S3).

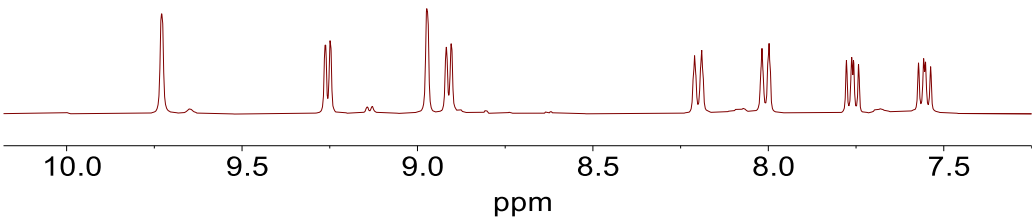

Figure S2. ^{1}H NMR spectrum (400 MHz, CD_3CN) of $[Pd_4(\mathbf{L2})_8](BF_4)_8$. The spectrum indicates the presence of small amounts of another species. According to the MS data (Figure S5), this species is a $[Pd_3(\mathbf{L2})_6]^{6+}$ complex.

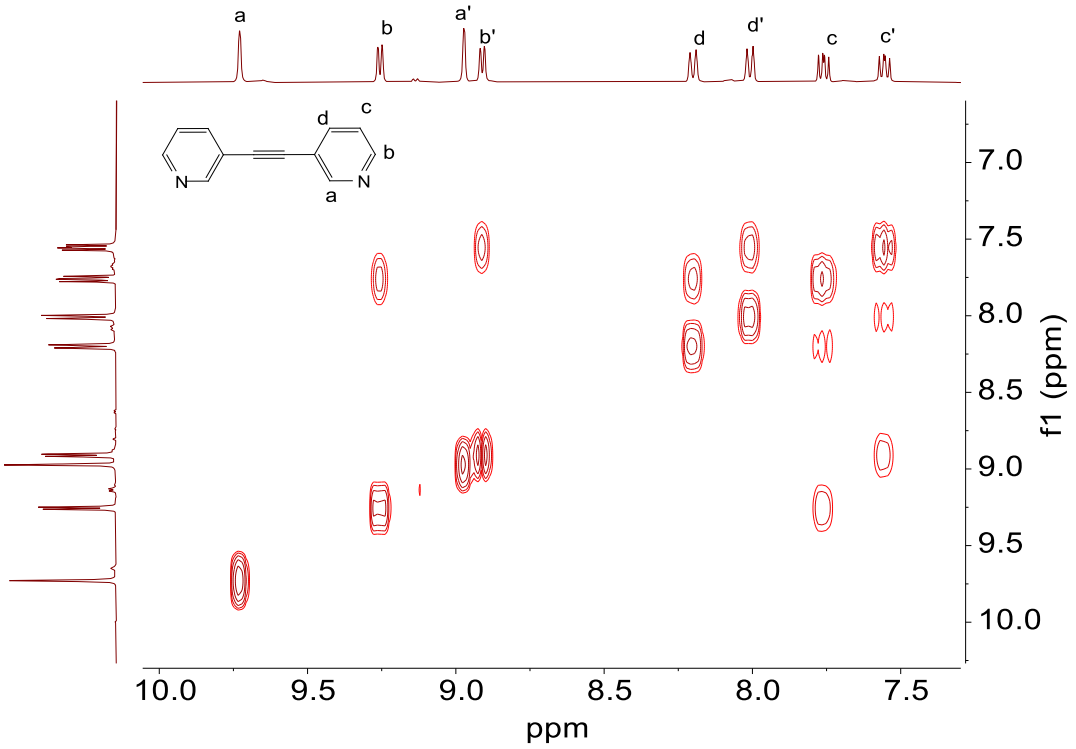

Figure S3. ^{1}H-^{1}H COSY NMR spectrum (400 MHz, CD_3CN) of $[Pd_4(\mathbf{L2})_8](BF_4)_8$.

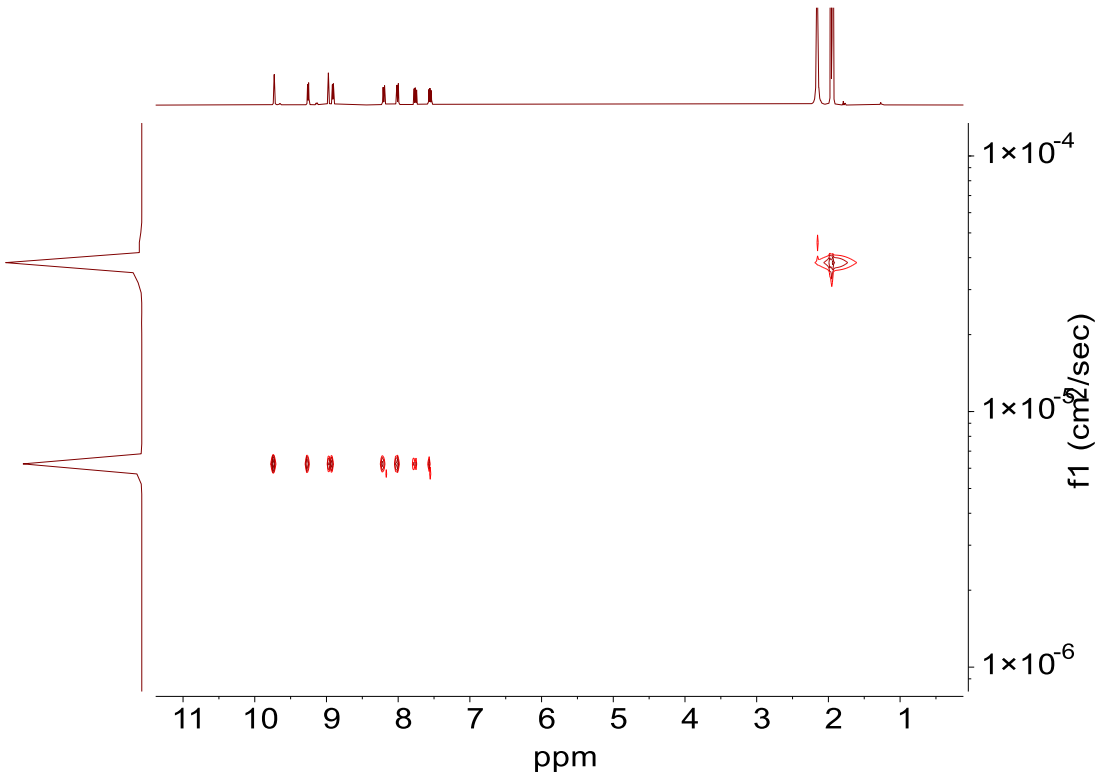

Figure S4. ^{1}H-^{1}H DOSY NMR spectrum (400 MHz, CD_3CN) of $[Pd_4(\mathbf{L2})_8](BF_4)_8$ (D = 6.26 x 10^{-10} m^2 s^{-1}).

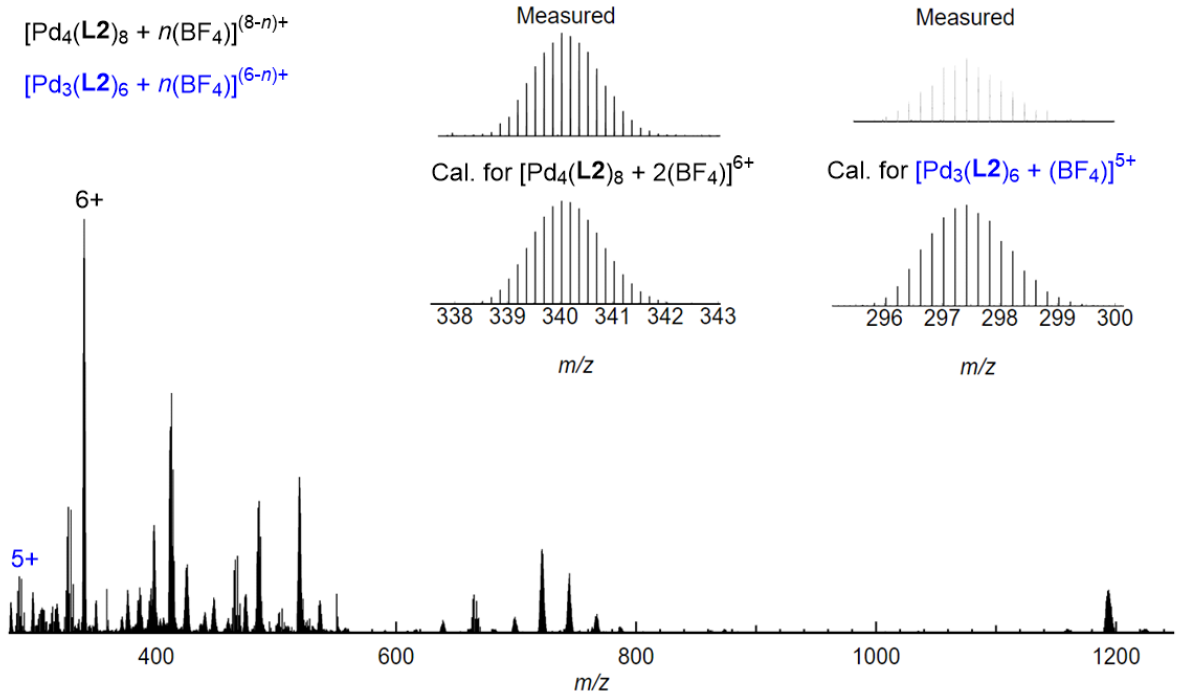

Figure S5. High-resolution ESI mass spectrum of $[Pd_4(\mathbf{L2})_8+2BF_4]^{6+}$. Small peaks, which can be attributed to a species of the formula $[Pd_3(\mathbf{L2})_6+ BF_4]^{5+}$, can be detected.

2.2. Synthesis of $[Pd_4(\mathbf{L2})_4(\mathbf{L3})_4](BF_4)_8$

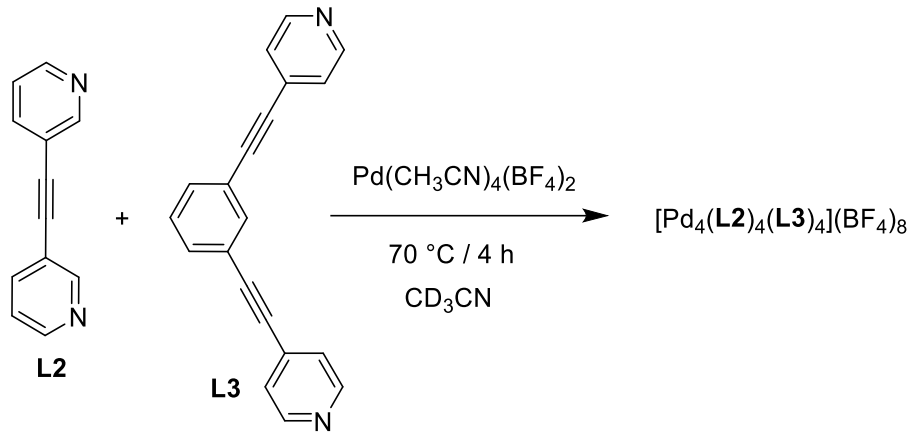

A solution of $[Pd(CH_3CN)_4](BF_4)_2$ (9 µmol, 300 µL of a 30 mM stock solution in CH_3CN) was combined with a 1:1 mixture of ligand **L2** (9 µmol, 100 µL of a 90 mM stock solution of **L2** in CH_3CN) and **L3** (9 µmol, 100 µL of a 90 mM stock solution of **L3** in CH_3CN) in 500 µL CH_3CN at 70 °C for 4 h. The reaction was cooled down to room temperature and diethyl ether (around 10 mL) was added. The resulting precipitate was isolated by centrifugation, washed with diethyl ether, and dried under vacuum to give the $[Pd_4(\mathbf{L2})_4(\mathbf{L3})_4](BF_4)_8$ (5.9 mg, 2.0 µmol, 89%). ^{1}H NMR (400 MHz, CD_3CN) δ 10.03 (d, *J* = 1.8 Hz, 8H), 9.10 – 9.06 (m, 16H), 9.04 (dd, *J* = 5.9, 1.3 Hz, 8H), 8.02 (dt, *J* = 8.1, 1.5 Hz, 8H), 7.89 (t, *J* = 1.7 Hz, 4H), 7.73 – 7.68 (m, 16H), 7.68 – 7.60 (m, 16H), 7.56 – 7.49 (m, 4H) (for an assignment of the signals, see Figure S7).

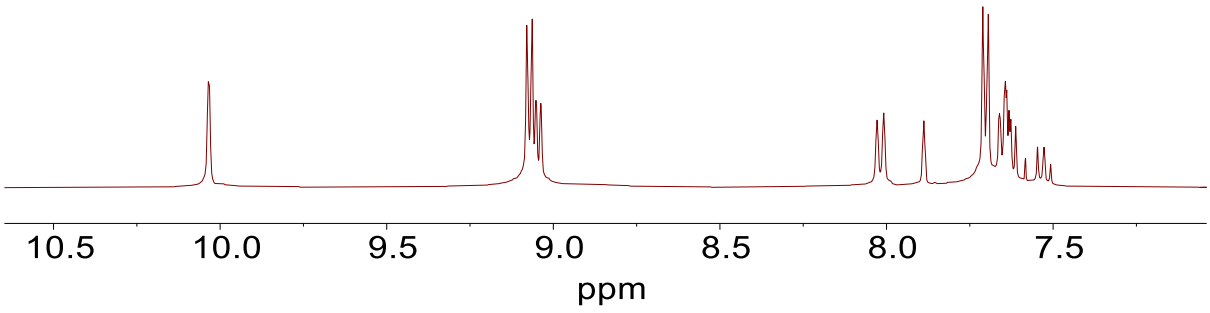

Figure S6. ^{1}H NMR spectrum (400 MHz, CD_3CN) of $[Pd_4(\mathbf{L2})_4(\mathbf{L3})_4](BF_4)_8$.

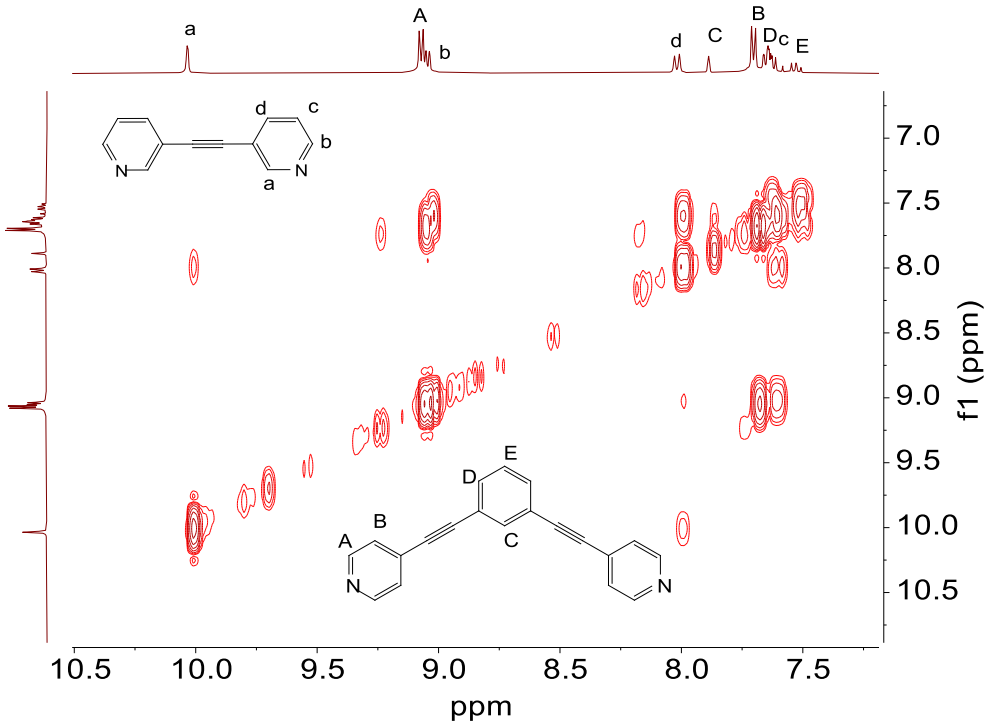

Figure S7. ^{1}H-^{1}H COSY NMR spectrum (400 MHz, CD_3CN) of $[Pd_4(\mathbf{L2})_4(\mathbf{L3})_4](BF_4)_8$.

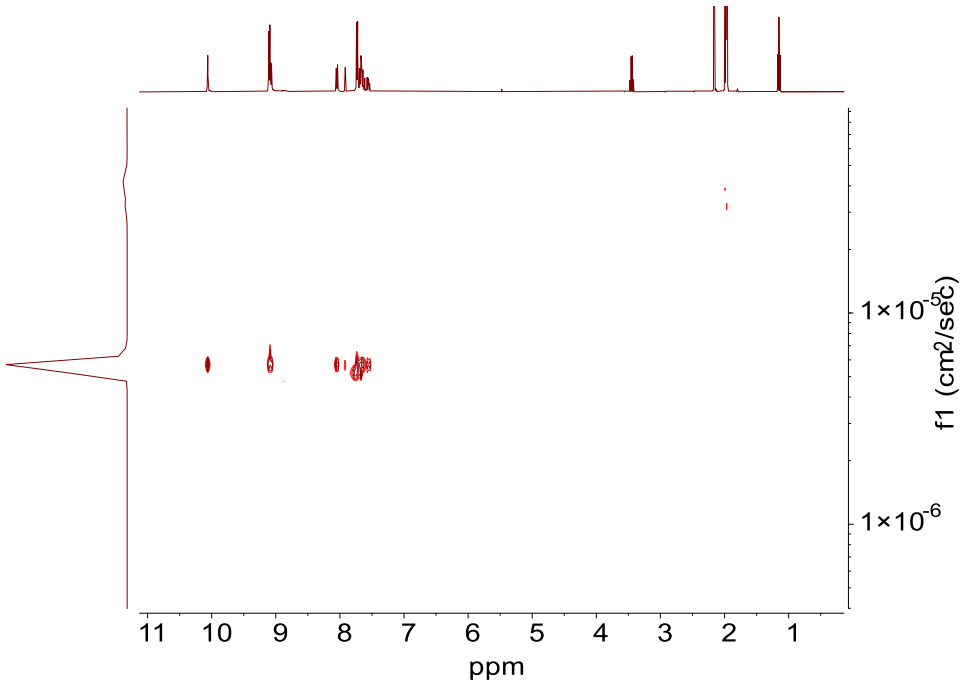

Figure S8. ^{1}H-^{1}H DOSY NMR spectrum (400 MHz, CD_3CN) of $[Pd_4(\mathbf{L2})_4(\mathbf{L3})_4](BF_4)_8$.
(D = 5.71 x 10^{-10} m^2 s^{-1}).

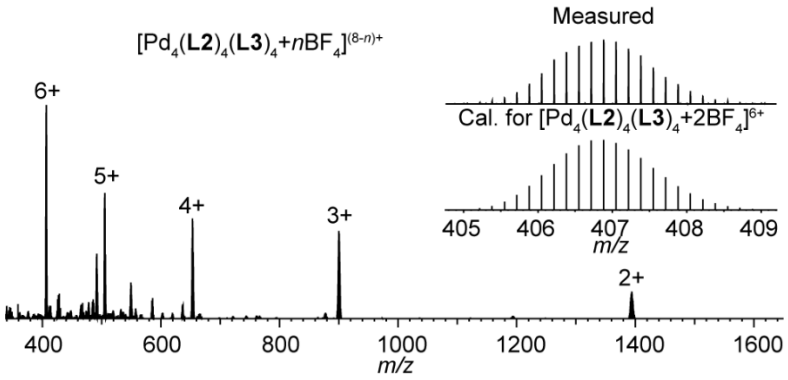

Figure S9. High-resolution ESI mass spectrum of $[Pd_4(\mathbf{L2})_4(\mathbf{L3})_4+n BF_4]^{(8-n)+}$ (n = 2 – 6).

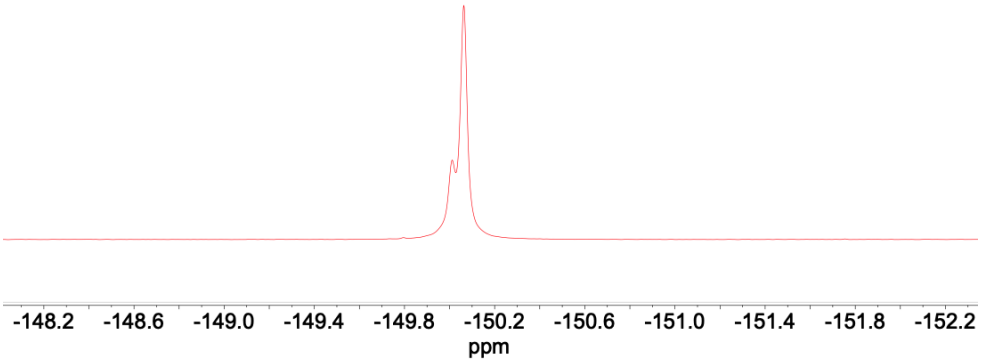

Figure S10. ^{19}F NMR spectrum of $[Pd_2(\mathbf{L2})_2(\mathbf{L3})_2](BF_4)_4$. The smaller peak at –150.0 ppm can be attributed to encapsulated BF_4^-.

2.3. Synthesis of $[Pd_2(\mathbf{L1'})_2(\mathbf{L2})_2](BF_4)_4$

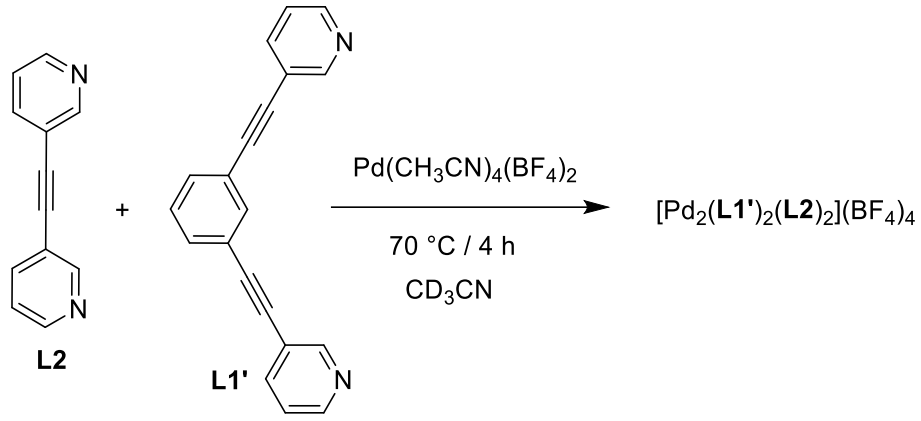

The cage $[Pd_2(\mathbf{L1'})_2(\mathbf{L2})_2](BF_4)_4$ was synthesized by stirring a mixture of ligand **L2** (4.5 µmol, 100 µL of a 45 mM stock solution of **L2** in CD_3CN), **L1'** (4.5 µmol, 100 µL of a 45 mM stock solution of **L1'** in CD_3CN), and $[Pd(CH_3CN)_4](BF_4)_2$ (4.5 µmol, 150 µL of a 30 mM stock solution in CD_3CN) in 650 µL CD_3CN at 70 °C for 4 h to give 1000 µL of a 2.25 mM solution of cage $[Pd_2(\mathbf{L1'})_2(\mathbf{L2})_2](BF_4)_4$. ^1H NMR (400 MHz, CD_3CN) δ 10.02 (d, *J* = 1.8 Hz, 4H), 9.38 (d, *J* = 1.8 Hz, 4H), 9.13 (dd, *J* = 5.8, 1.3 Hz, 4H), 8.98 (dd, *J* = 5.9, 1.3 Hz, 4H), 8.20 (dt, *J* = 1.7, 0.9 Hz, 2H), 8.02 (tt, *J* = 8.3, 1.5 Hz, 8H), 7.68 (ddd, *J* = 8.0, 5.8, 0.7 Hz, 4H), 7.64 – 7.54 (m, 8H), 7.49 (ddd, *J* = 8.5, 6.9, 0.6 Hz, 2H)) (for an assignment of the signals, see Figure S12).

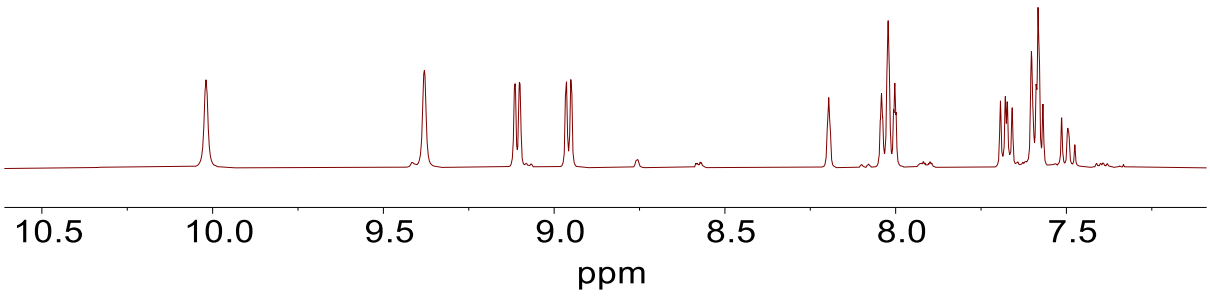

Figure S11. ^1H NMR spectrum (400 MHz, CD_3CN) of $[Pd_2(\mathbf{L1'})_2(\mathbf{L2})_2](BF_4)_4$.

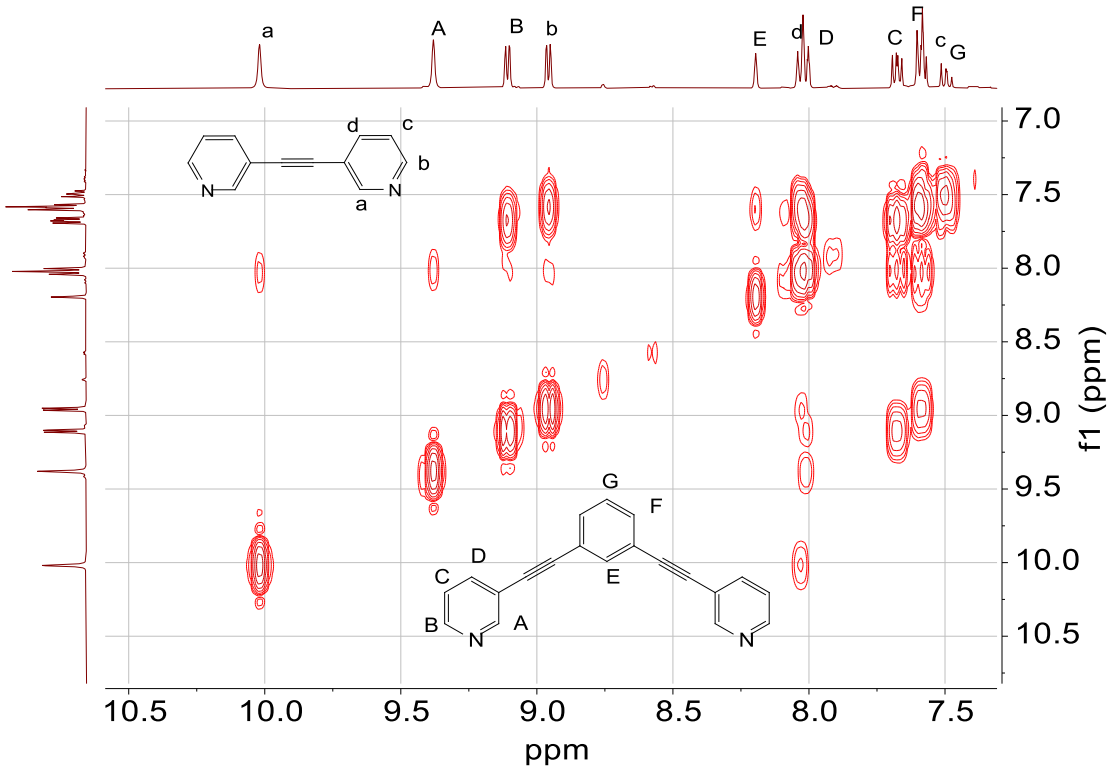

Figure S12. ^{1}H-^{1}H COSY NMR spectrum (400 MHz, CD_3CN) of $[Pd_2(\mathbf{L1'})_2(\mathbf{L2})_2](BF_4)_4$.

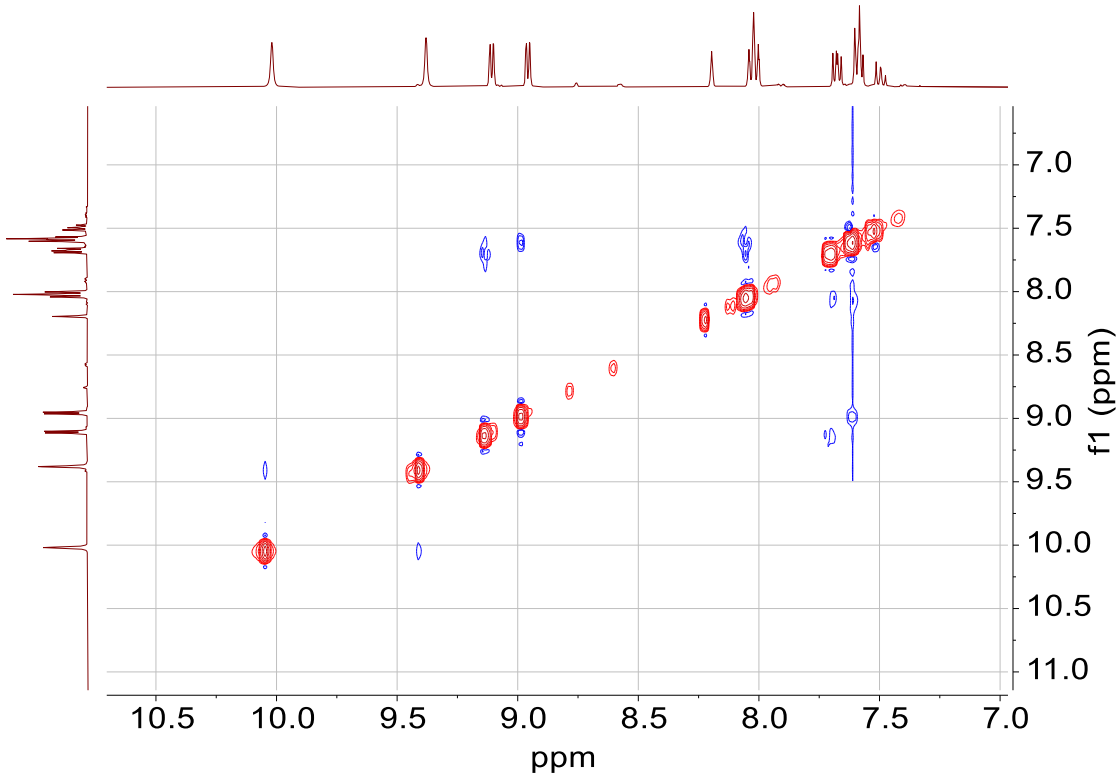

Figure S13. ^{1}H-^{1}H COSY NMR spectrum (400 MHz, CD_3CN) of $[Pd_2(\mathbf{L1'})_2(\mathbf{L2})_2](BF_4)_4$.

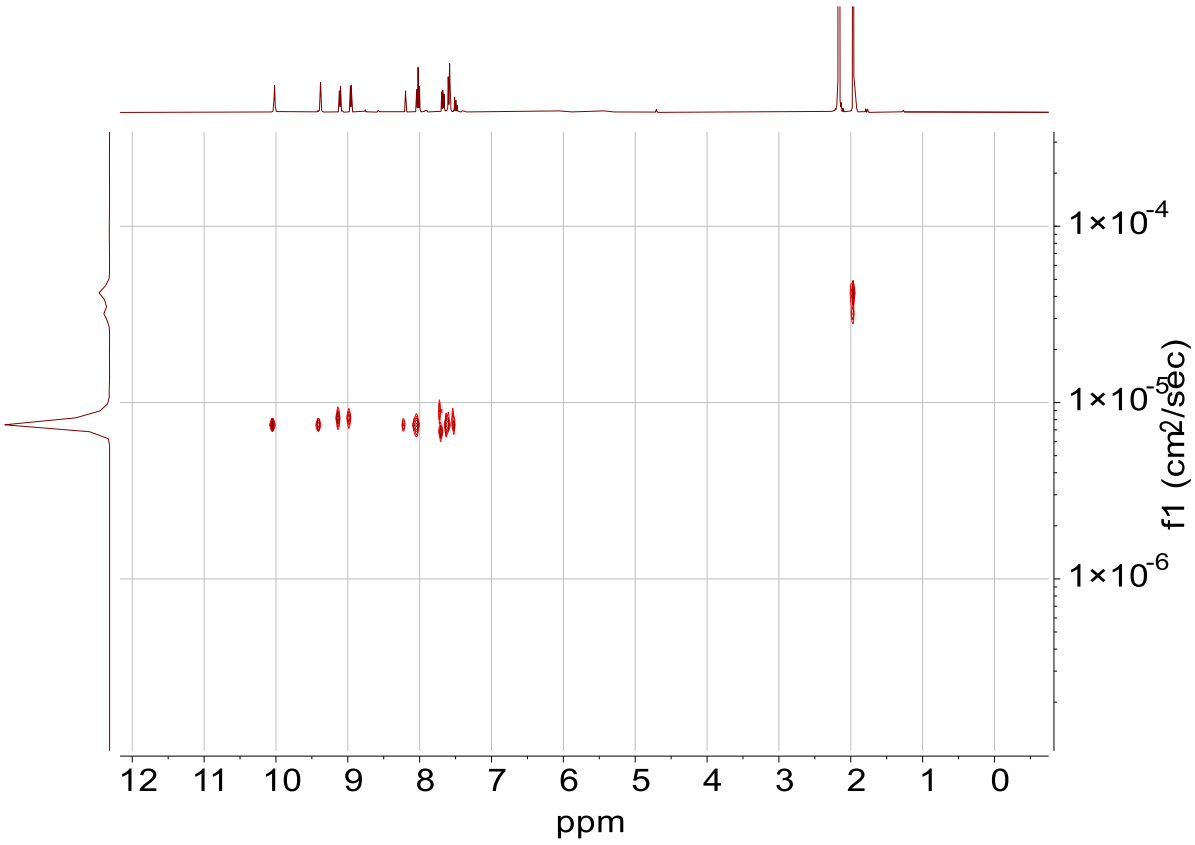

Figure S14. ^{1}H-^{1}H DOSY NMR spectrum (400 MHz, CD_3CN) of $[Pd_2(\mathbf{L1'})_2(\mathbf{L2})_2](BF_4)_4$. ($D$ = 7.50 x 10^{-10} m^2 s^{-1}).

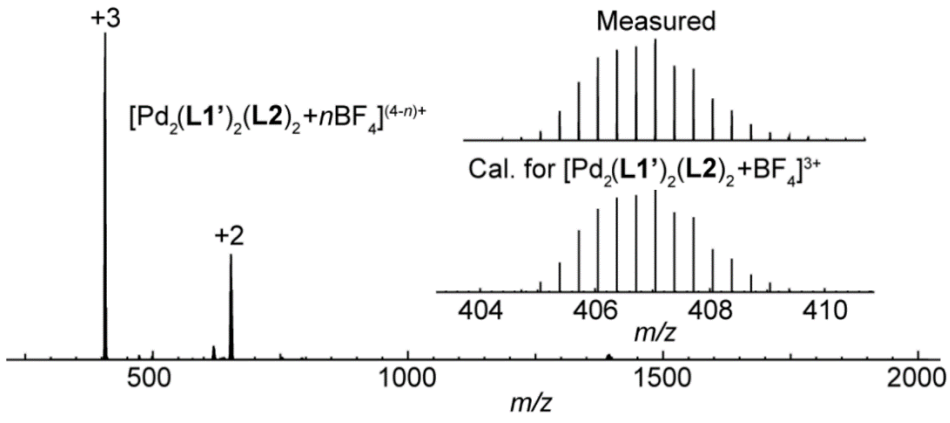

Figure S15. High-resolution ESI mass spectrum of $[Pd_2(\mathbf{L1'})_2(\mathbf{L2})_2+nBF_4]^{(4-n)+}$ (n = 1 or 2).

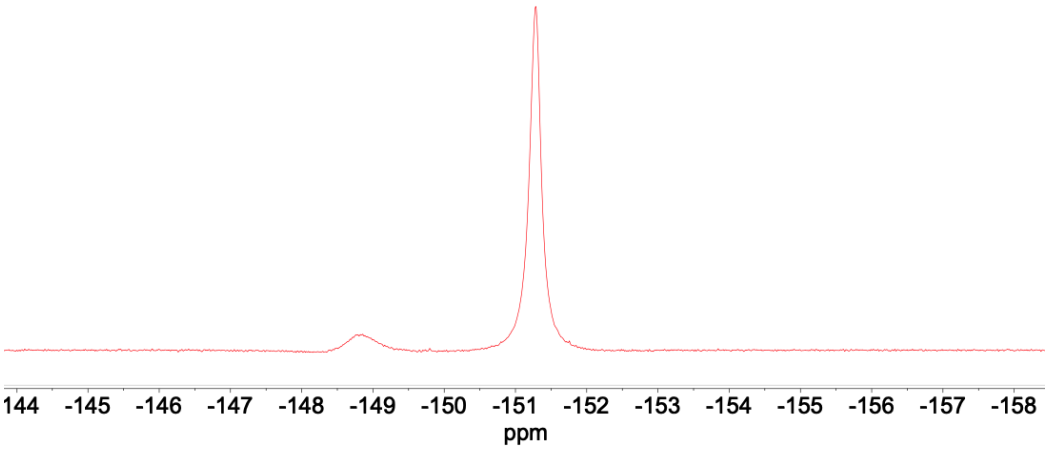

Figure S16. ^{19}F NMR spectrum of $[Pd_2(\mathbf{L1'})_2(\mathbf{L2})_2](BF_4)_4$. The smaller peak at –149 ppm points to the presence of encapsulted BF_4^-.

3. Additional combinations of two ligands

The cages were prepared in NMR tubes from mixtures of ligands **L1** (4.5 μmol, 50 μL of a 90 mM solution in CD_3CN), **L1'** (4.5 μmol, 50 μL of a 90 mM solution in CD_3CN), **L2** (4.5 μmol, 50 μL of a 90 mM solution in CD_3CN), **L2'** (4.5 μmol, 50 μL of a 90 mM solution in CD_3CN), **L3** (4.5 μmol, 100 μL of a 45 mM solution in CD_3CN), or **L3'** (4.5 μmol, 100 μL of a 45 mM solution in CD_3CN) and $[Pd(CH_3CN)_4](BF_4)_2$ (4.5 μmol, 150 μL of a 30 mM stock solution in CD_3CN) in 200 μL or 250 μL CD_3CN and heated at 70 °C overnight to give 500 μL of cage solutions.

3.1. Combination of **L2** + **L3'**

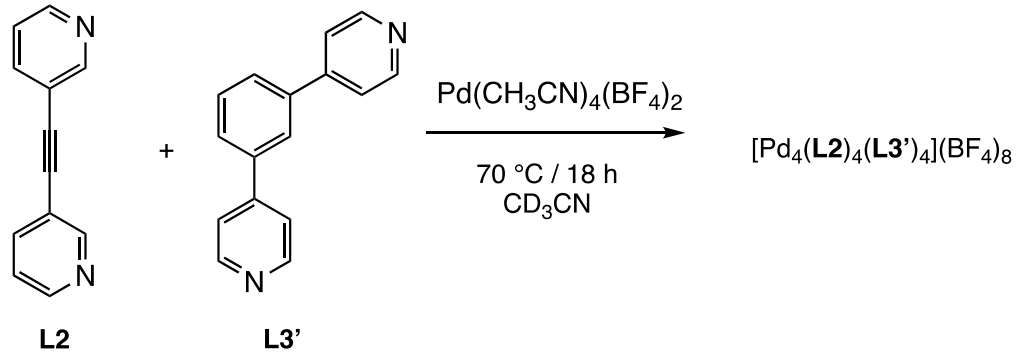

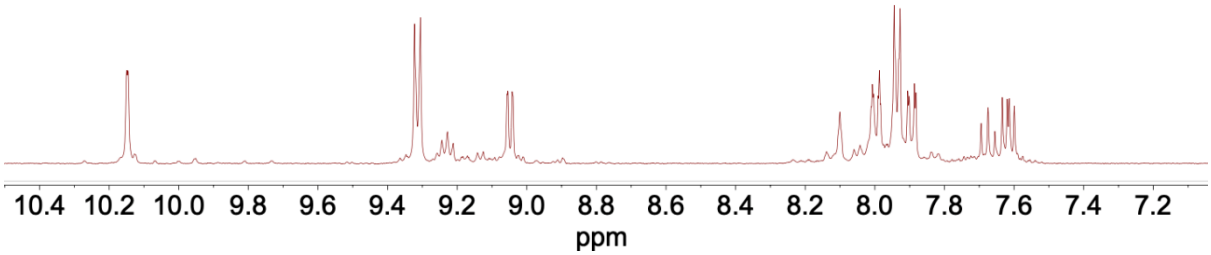

Figure S17. ^{1}H NMR spectrum (400 MHz, CD_3CN) of an equilibrated mixture containing $[Pd(CH_3CN)_4](BF_4)_2$ and the ligands **L2** and **L3'** (1:1:1).

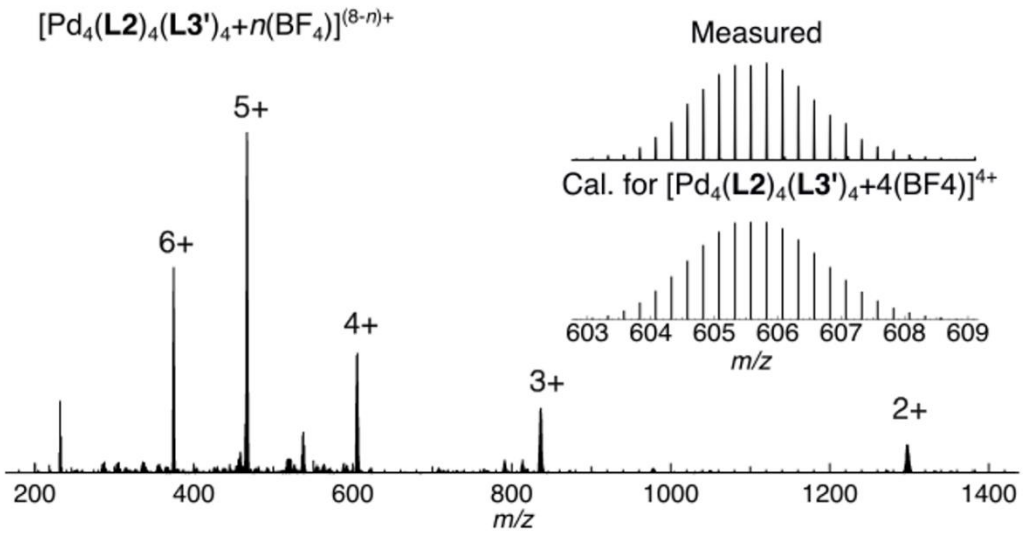

Figure S18. High-resolution ESI mass spectrum of an equilibrated mixture containing $[Pd(CH_3CN)_4](BF_4)_2$ and the ligands **L2** and **L3'** (1:1:1). The main peaks can be attributed to species with the formula $[Pd_4(\mathbf{L2})_4(\mathbf{L3'})_4 + n(BF_4)]^{(8-n)+}$.

3.2. Combination of **L1'** + **L3**

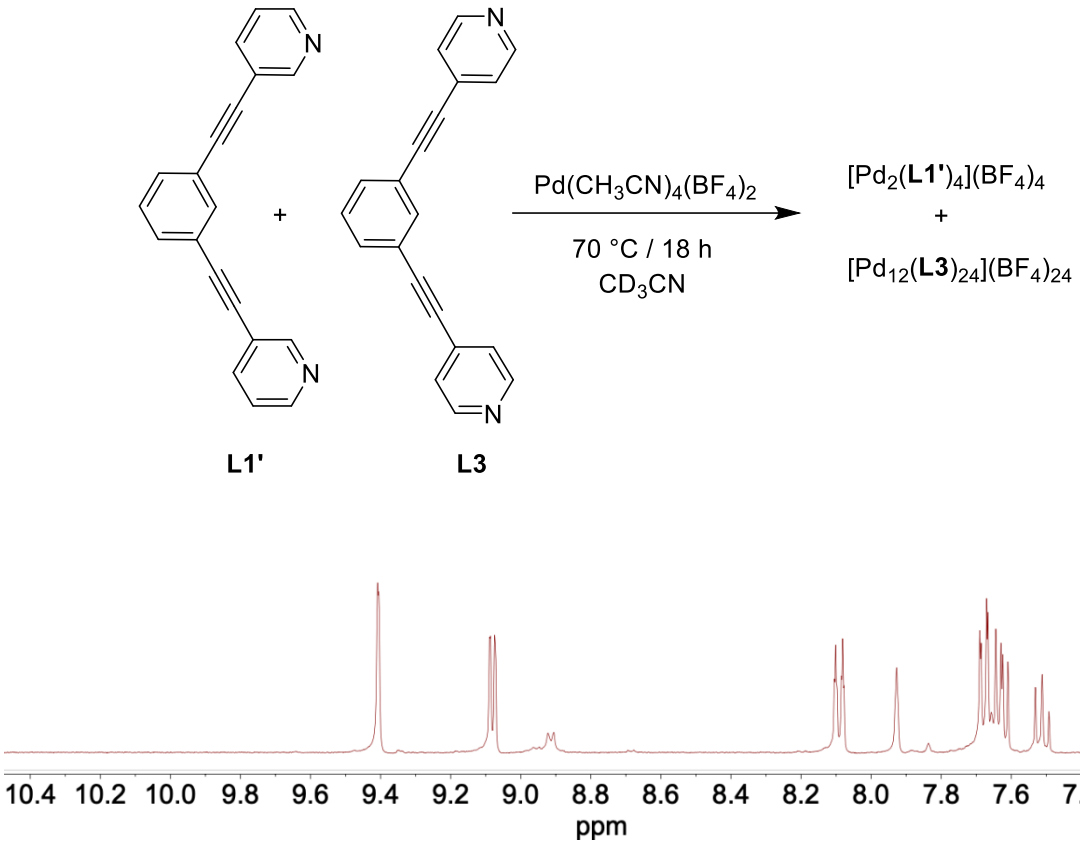

Figure S19. ^{1}H NMR spectrum (400 MHz, CD_3CN) of an equilibrated mixture containing $[Pd(CH_3CN)_4](BF_4)_2$ and the ligands **L1'** and **L3**.

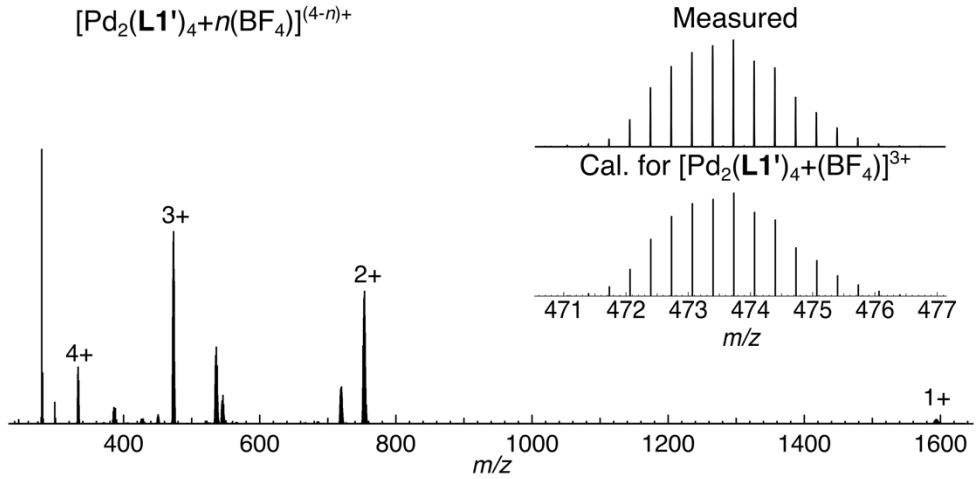

Figure S20. High-resolution ESI mass spectrum of an equilibrated mixture containing $[Pd(CH_3CN)_4](BF_4)_2$ and the ligands **L1'** and **L3** (1:1:1). Main peaks can be attributed to species with the formula $[Pd_2(\mathbf{L1'})_4 + n(BF_4)]^{(8-n)+}$.

3.3. Combination of **L1'** + **L2'**

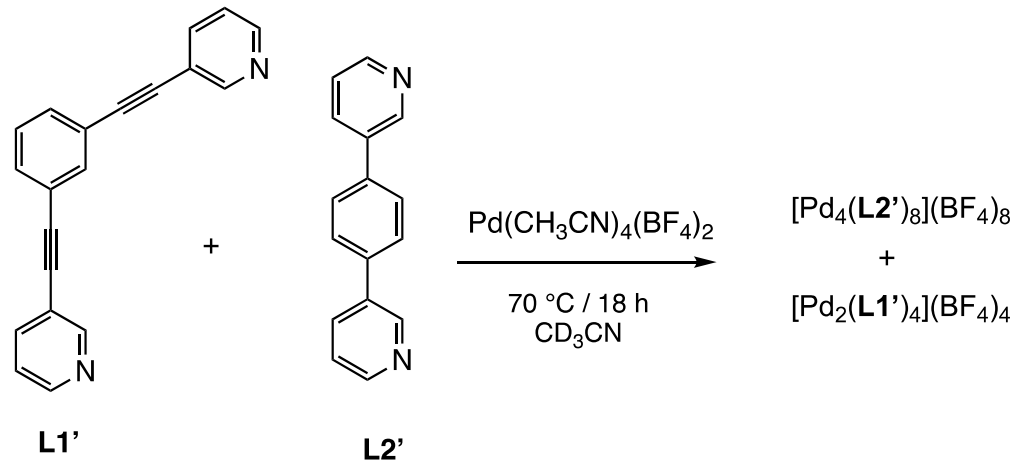

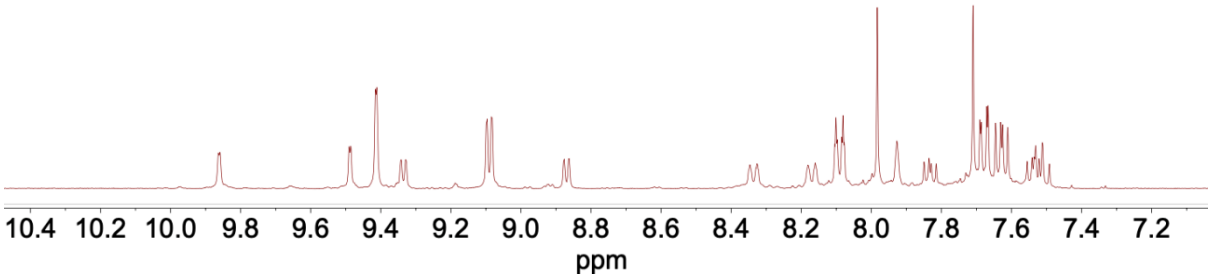

Figure S21. ^{1}H NMR spectrum (400 MHz, CD_3CN) of an equilibrated mixture containing $[Pd(CH_3CN)_4](BF_4)_2$ and the ligands **L1'** and **L2'** (1:1:1).

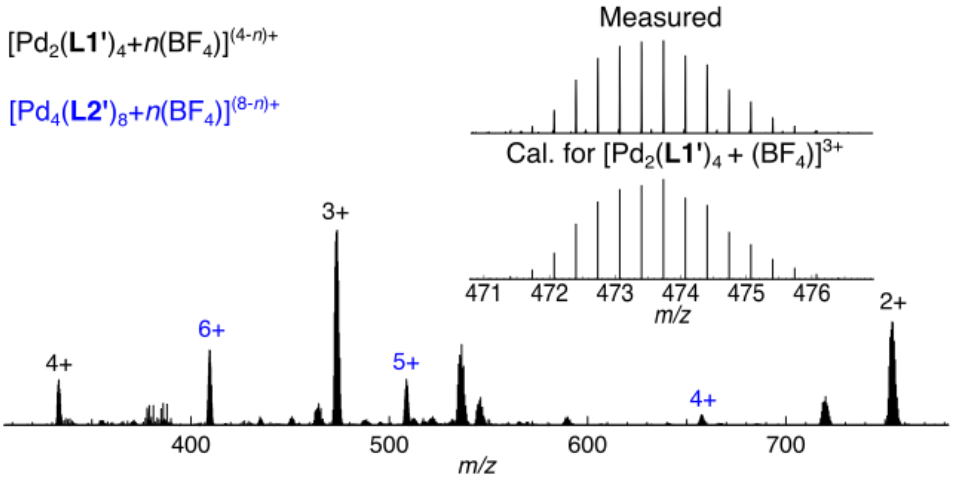

Figure S21. High-resolution ESI mass spectrum of an equilibrated mixture containing $[Pd(CH_3CN)_4](BF_4)_2$ and the ligands **L1'** and **L2'** (1:1:1). Main peaks can be attributed to species with the formula $[Pd_2(\mathbf{L1'})_4 + n(BF_4)]^{(4-n)+}$ and $[Pd_4(\mathbf{L2'})_8 + n(BF_4)]^{(8-n)+}$.

3.4. Combination of **L1** + **L2**

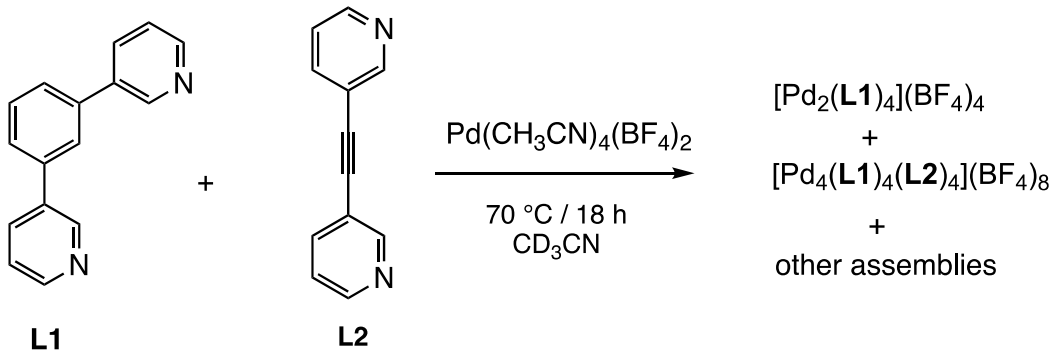

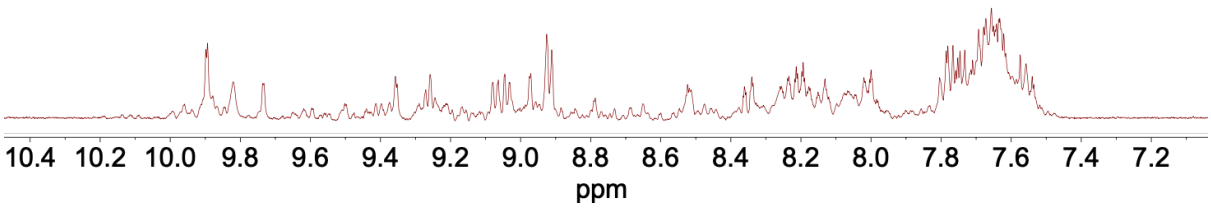

Figure S22. ^{1}H NMR spectrum (400 MHz, CD_3CN) of an equilibrated mixture containing $[Pd(CH_3CN)_4](BF_4)_2$ and the ligands **L1** and **L2** (1:1:1).

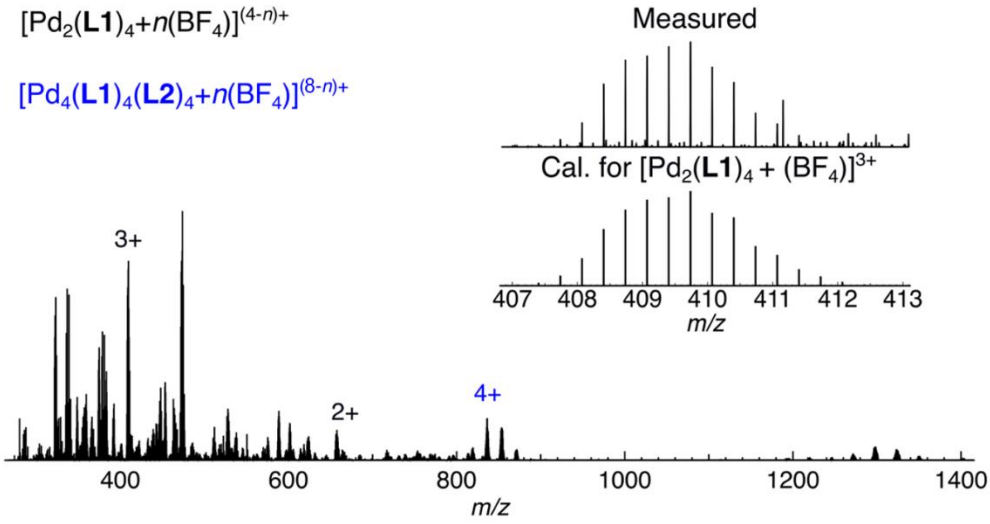

Figure S23. High-resolution ESI mass spectrum of an equilibrated mixture containing $[Pd(CH_3CN)_4](BF_4)_2$ and the ligands **L1** and **L2** (1:1:1). Peaks can be attributed to species with the formula $[Pd_2(\mathbf{L1})_4 + n(BF_4)]^{(4-n)+}$ and $[Pd_4(\mathbf{L1})_4(\mathbf{L2})_4 + n(BF_4)]^{(8-n)+}$.

3.5. Combination of **L1** + **L2'**

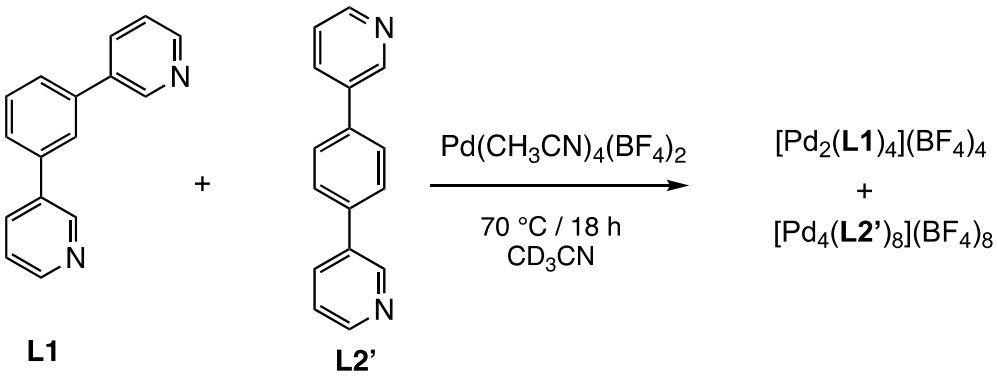

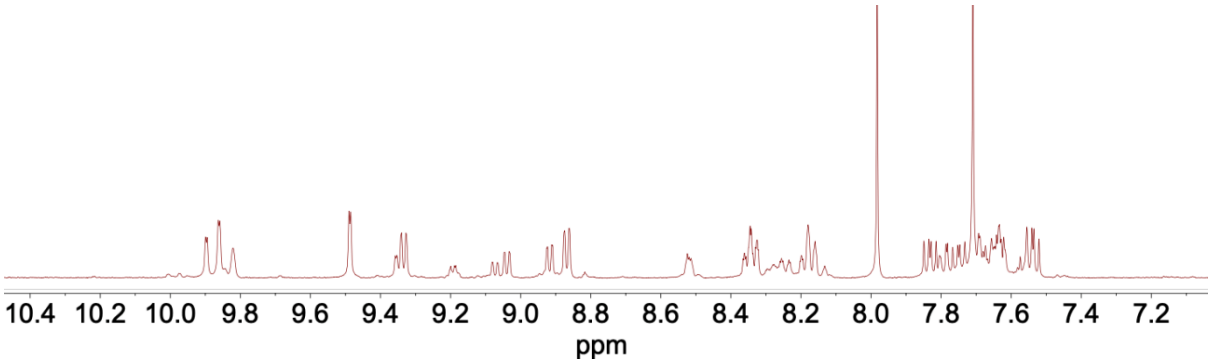

Figure S24. ^{1}H NMR spectrum (400 MHz, CD_3CN) of an equilibrated mixture containing $[Pd(CH_3CN)_4](BF_4)_2$ and the ligands **L1** and **L2'** (1:1:1).

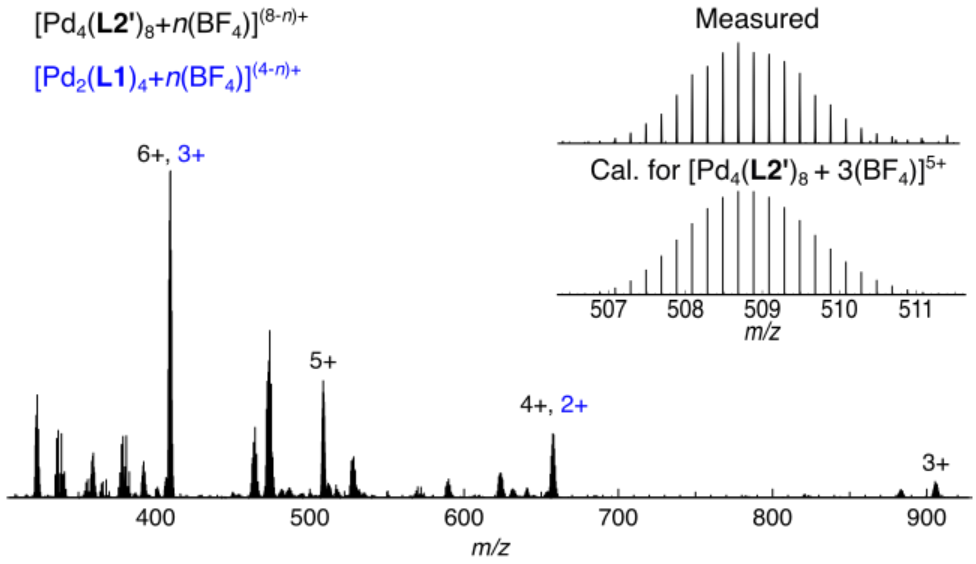

Figure S25. High-resolution ESI mass spectrum of an equilibrated mixture containing $[Pd(CH_3CN)_4](BF_4)_2$ and the ligands **L1** and **L2'** (1:1:1). Main peaks can be attributed to species with the formula $[Pd_2(\mathbf{L1})_4 + n(BF_4)]^{(4-n)+}$ and $[Pd_4(\mathbf{L2'})_8 + n(BF_4)]^{(8-n)+}$.

3.6. Combination of **L1** + **L3**

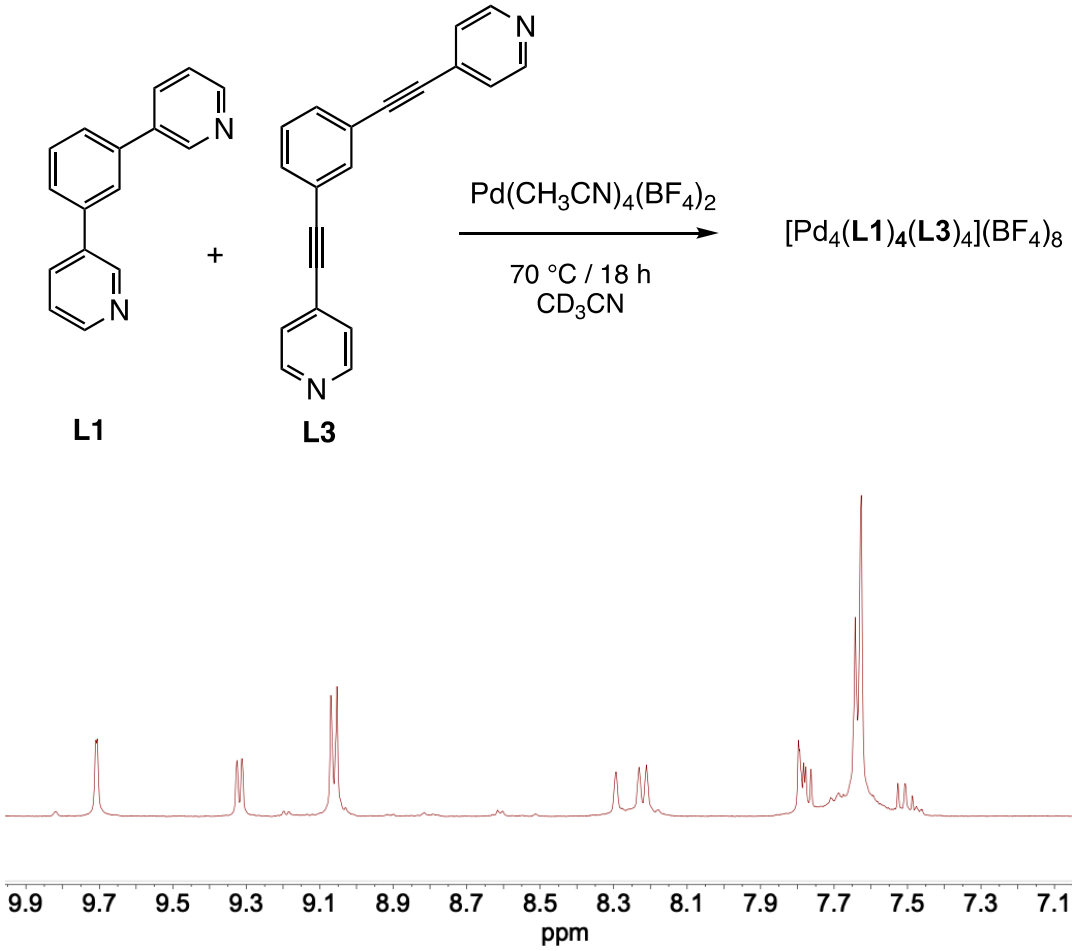

Figure S26. ^{1}H NMR spectrum (400 MHz, CD_3CN) of an equilibrated mixture containing $[Pd(CH_3CN)_4](BF_4)_2$ and the ligands **L1** and **L3** (1:1:1).

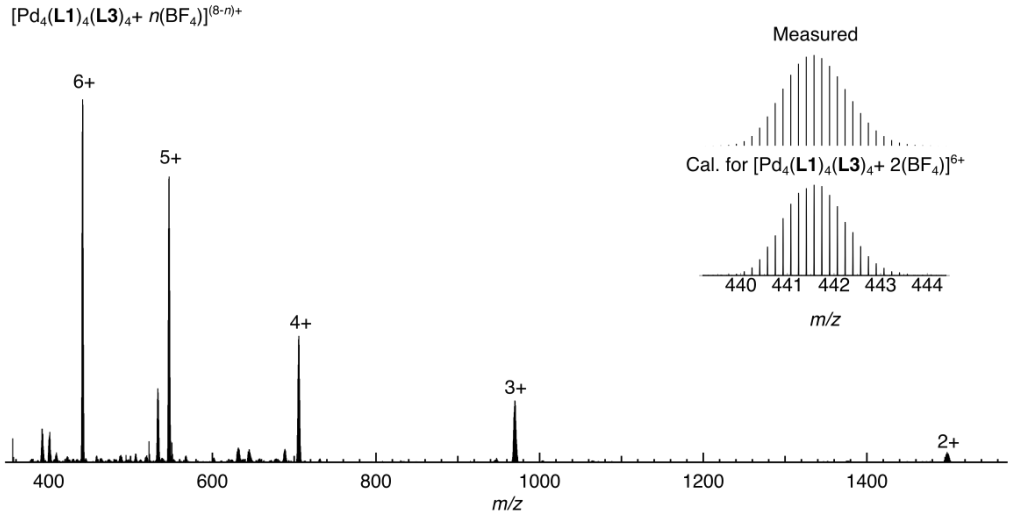

Figure S27. High-resolution ESI mass spectrum of an equilibrated mixture containing $[Pd(CH_3CN)_4](BF_4)_2$ and the ligands **L1** and **L3** (1:1:1). The main peaks can be attributed to species of the formula $[Pd_4(\mathbf{L1})_4(\mathbf{L3})_4 + n(BF_4)]^{(8-n)+}$.

3.7. Combination of **L1** + **L3'**

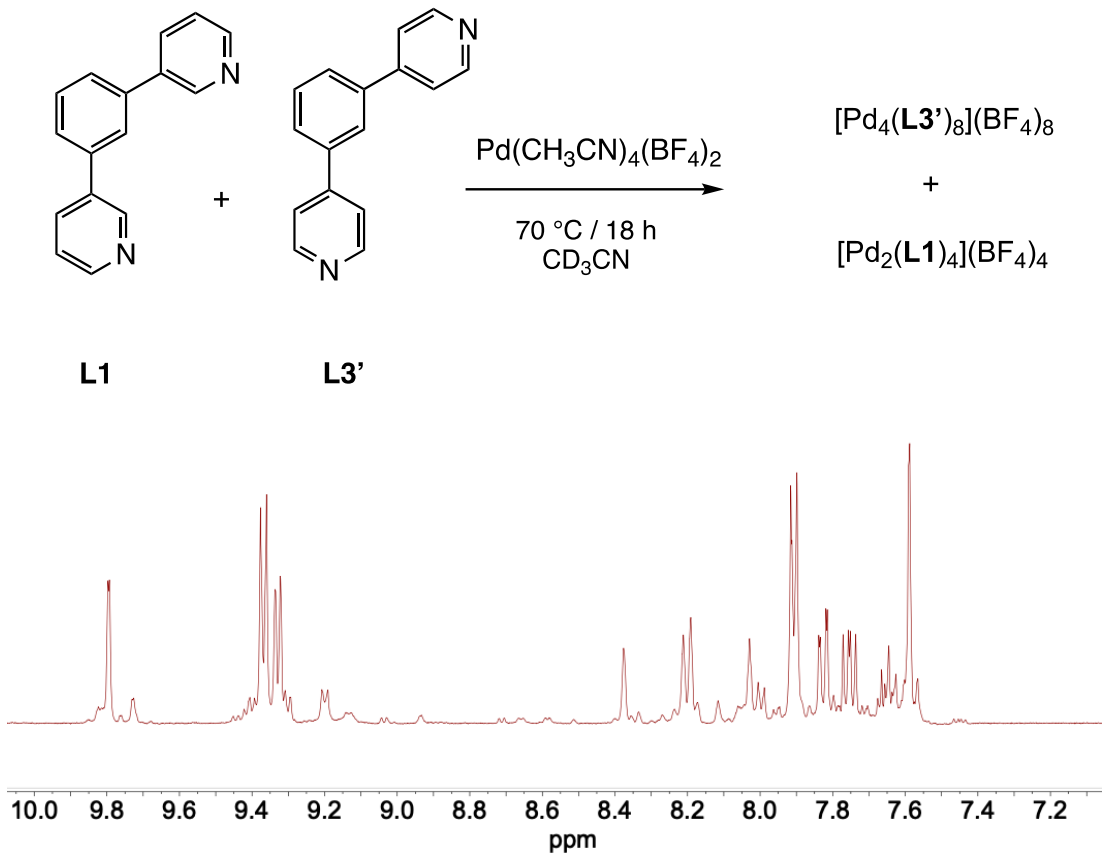

Figure S28. ^{1}H NMR spectrum (400 MHz, CD_3CN) of of an equilibrated mixture containing $[Pd(CH_3CN)_4](BF_4)_2$ and the ligands **L1** and **L3'** (1:1:1).

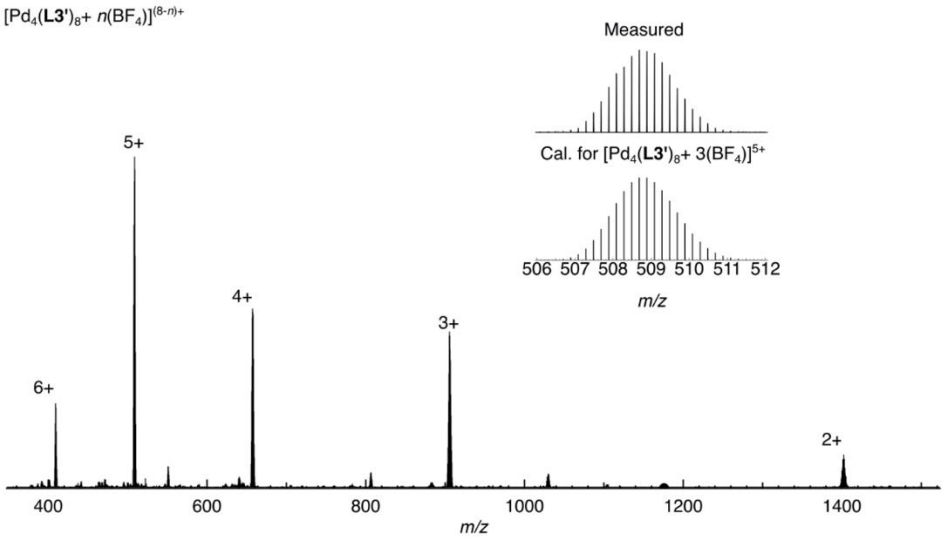

Figure S29. High-resolution ESI mass spectrum of an equilibrated mixture containing $[Pd(CH_3CN)_4](BF_4)_2$ and the ligands **L1** and **L3'** (1:1:1). The main peaks can be attributed to species with the formula $[Pd_4(\mathbf{L3})_4 + n(BF_4)]^{(8-n)+}$ (note: **L1** and **L3** have the same mass).

3.8. Combination of **L2'** + **L3**

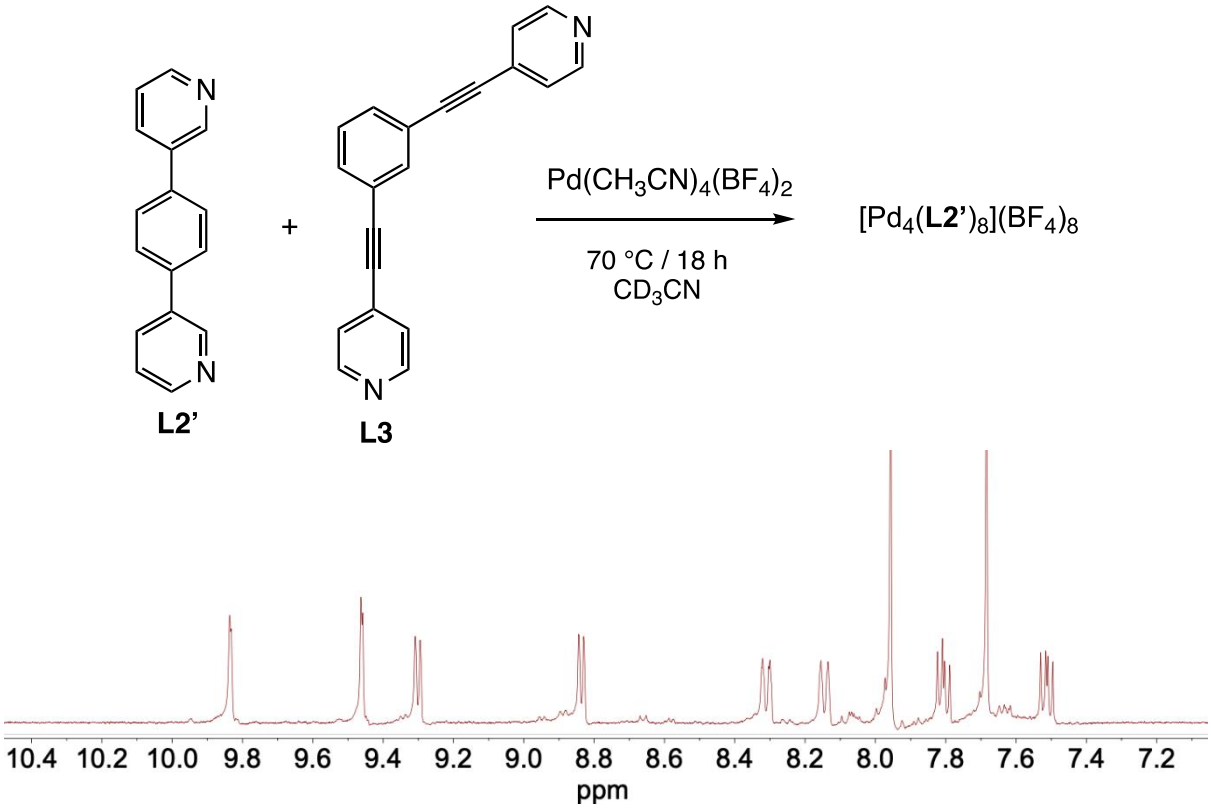

Figure S30. ^{1}H NMR spectrum (400 MHz, CD_3CN) of an equilibrated mixture containing $[Pd(CH_3CN)_4](BF_4)_2$ and the ligands **L2'** and **L3** (1:1:1).

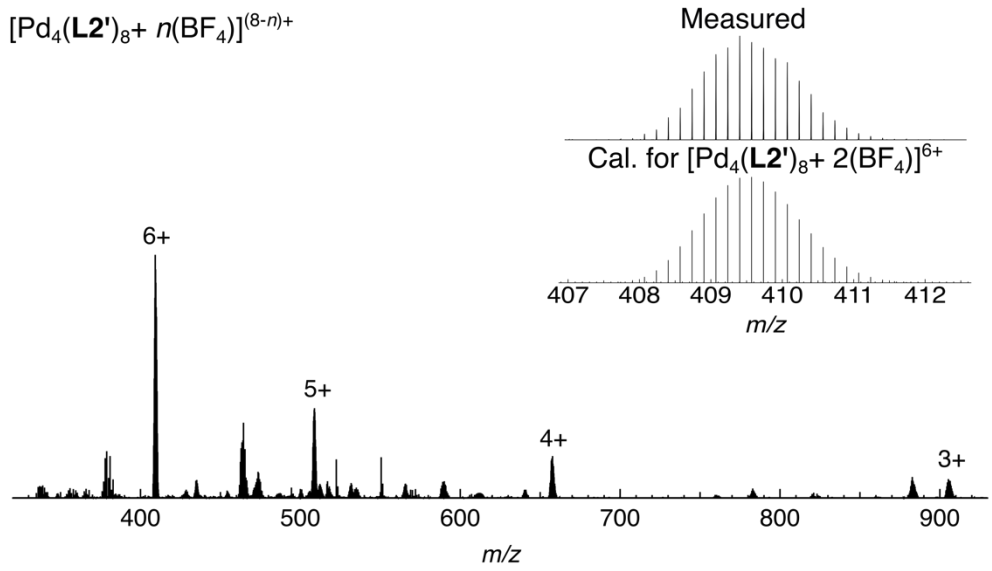

Figure S31. High-resolution ESI mass spectrum of an equilibrated mixture containing $[Pd(CH_3CN)_4](BF_4)_2$ and the ligands **L2** and **L3** (1:1:1). The main peaks can be attributed to species with the formula $[Pd_4(\mathbf{L2'})_4 + n(BF_4)]^{(8-n)+}$.

3.9. Combination of **L1'** + **L3'**

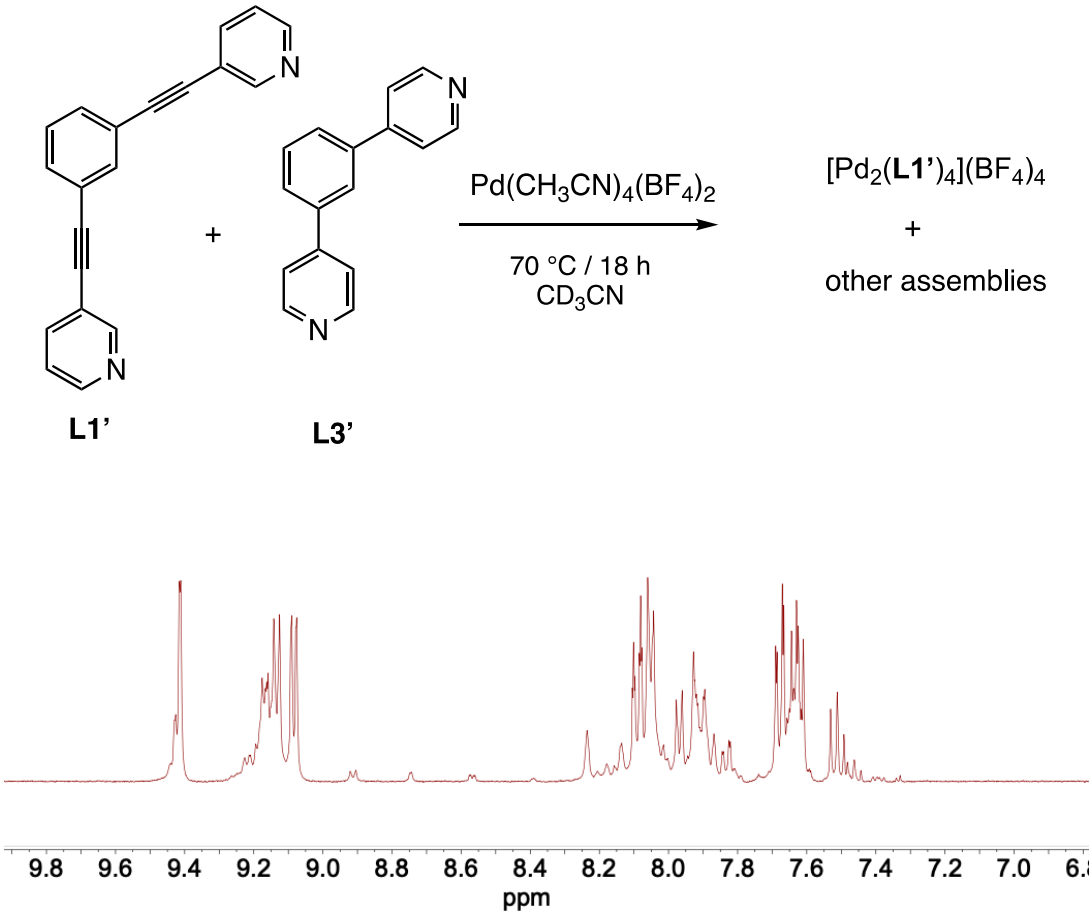

Figure S32. ^{1}H NMR spectrum (400 MHz, CD_3CN) of an equilibrated mixture containing $[Pd(CH_3CN)_4](BF_4)_2$ and the ligands **L1'** and **L3'** (1:1:1).

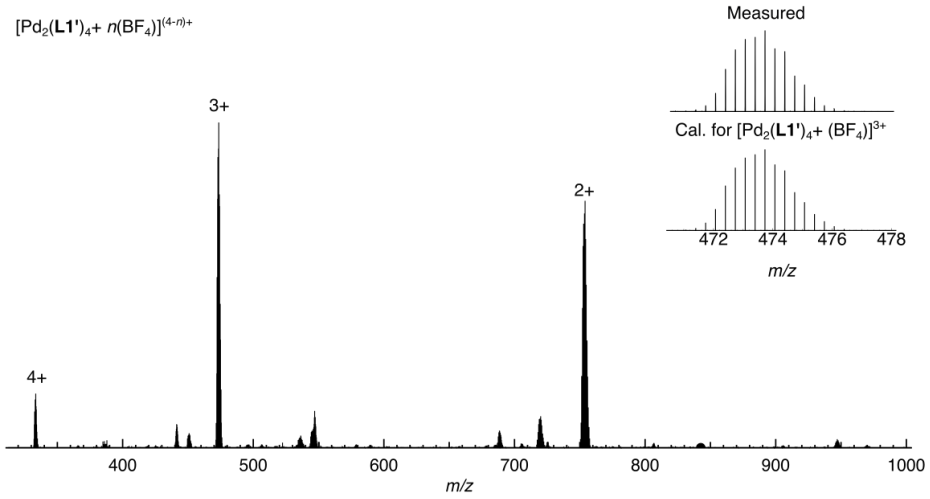

Figure S33. High-resolution ESI mass spectrum of an equilibrated mixture containing $[Pd(CH_3CN)_4](BF_4)_2$ and the ligands **L1'** and **L3'** (1:1:1). The main peaks can be attributed to species with the formula $[Pd_2(\mathbf{L1'})_4 + n(BF_4)]^{(4-n)+}$.

3.10 Combination of **L2'** + **L3'**

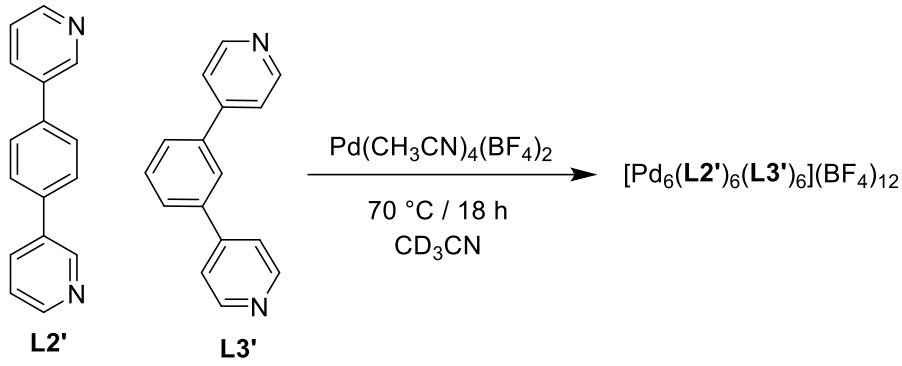

The combination of **L2'** and **L3'** has been investigated in a previous study.[S7] The reaction gives the hexanuclear complex $[Pd_6(\mathbf{L2'})_6(\mathbf{L3'})_6](BF_4)_{12}$.

4. Combinations of three ligands

The ligands **L1/L1'** (45 mM stock solution of **L1**/**L1'** in CD_3CN), **L2/L2'** (45 mM stock solution of **L2**/**L2'** in CD_3CN), **L3**/**L3'** (45 mM stock solution of **L3**/**L3'** in CD_3CN) were mixed in different ratio in CD_3CN, $[Pd(CH_3CN)_4](BF_4)_2$ (30 mM stock solution in CD_3CN) was added, and the ^1H NMR of the mixture was recorded after heating at 70 °C overnight.

4.1 Combination of **L1**, **L2** and **L3**

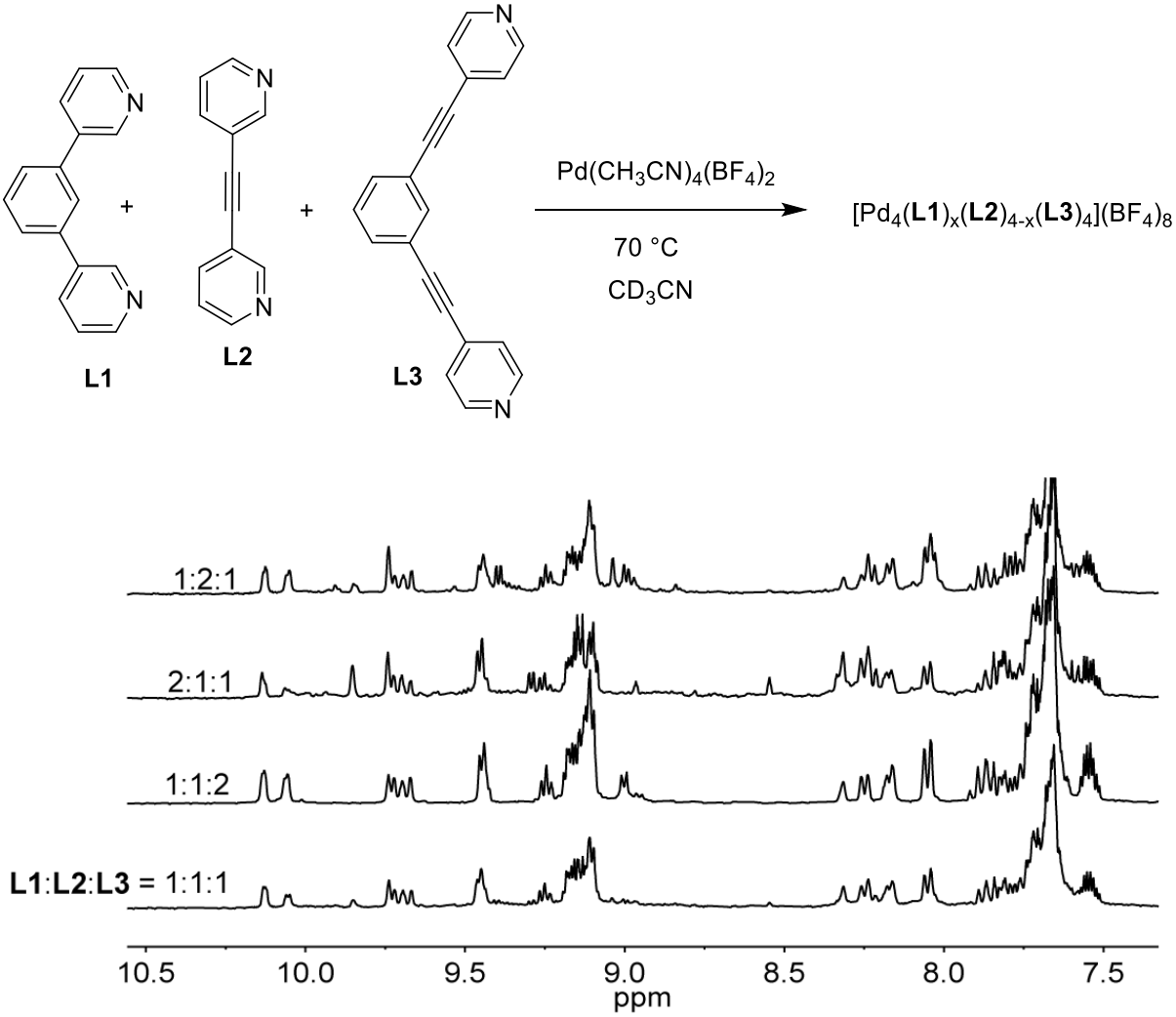

Figure S34. ^1H NMR spectra (400 MHz, CD_3CN) of equilibrated mixtures containing $[Pd(CH_3CN)_4](BF_4)_2$ and the ligands **L1**, **L2**, and **L3** in different ratios ($[\mathbf{L}]_{total}$: [Pd] = 2:1).

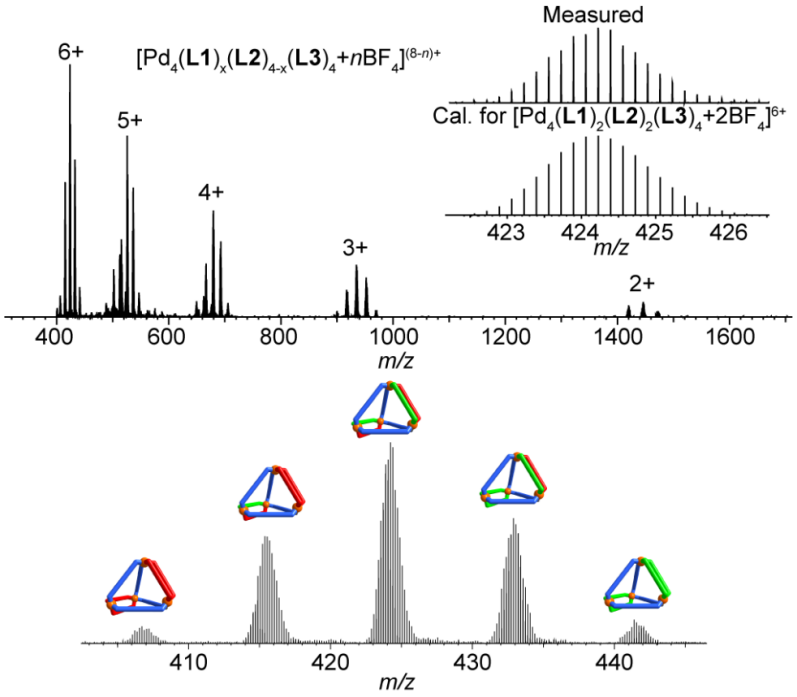

Figure S35. High-resolution ESI mass spectrum of an equilibrated mixture containing $[Pd(CH_3CN)_4](BF_4)_2$ and the ligands **L1**, **L2**, and **L3** (1:1:2; $[\mathbf{L}]_{total}$: [Pd] = 2:1.). Main peaks can be attributed to species of the formula $[Pd_4(\mathbf{L1})_x(\mathbf{L2})_{4-x}(\mathbf{L3})_4+n BF_4]^{(8-n)+}$ (n = 2 – 6, x = 0 – 4).

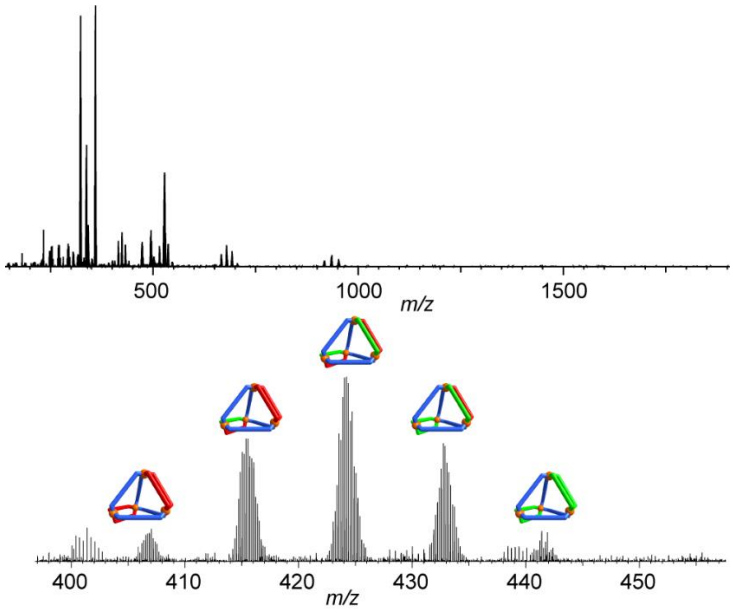

Figure S36. High-resolution ESI mass spectrum of an equilibrated mixture containing $[Pd(CH_3CN)_4](BF_4)_2$ and the ligands **L1**, **L2**, and **L3** (1:2:1; $[\mathbf{L}]_{total}$: [Pd] = 2:1.). Main peaks can be attributed to species of the formula $[Pd_4(\mathbf{L1})_x(\mathbf{L2})_{4-x}(\mathbf{L3})_4+n BF_4]^{(8-n)+}$ (n = 2 – 6, x = 0 – 4).

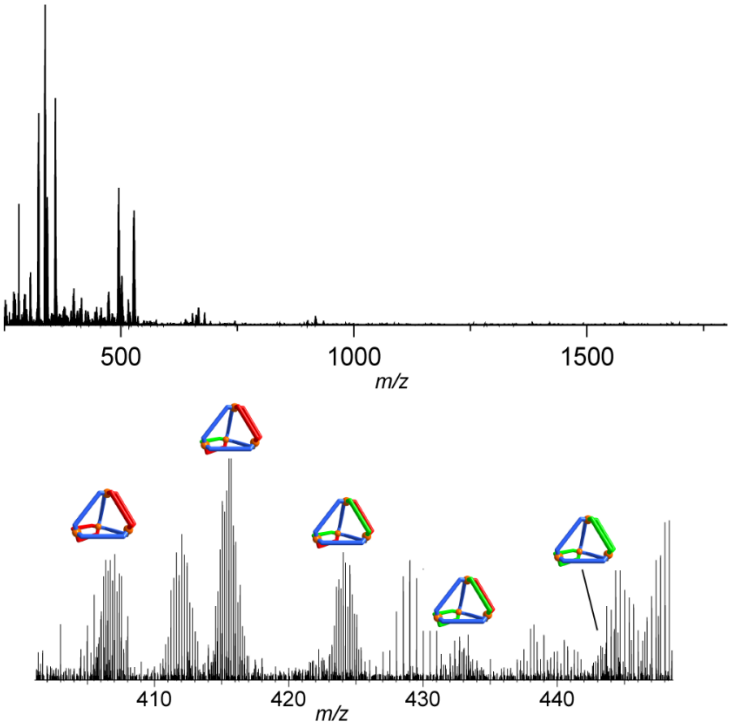

Figure S37. High-resolution ESI mass spectrum of an equilibrated mixture containing $[Pd(CH_3CN)_4](BF_4)_2$ and the ligands **L1**, **L2**, and **L3** (2:1:1; $[\mathbf{L}]_{total}$: [Pd] = 2:1.). Main peaks can be attributed to species of the formula $[Pd_4(\mathbf{L1})_x(\mathbf{L2})_{4-x}(\mathbf{L3})_4+n BF_4]^{(8-n)+}$ (n = 2 – 6, x = 0 – 4).

4.2 Combination of **L1'**, **L2** and **L3**

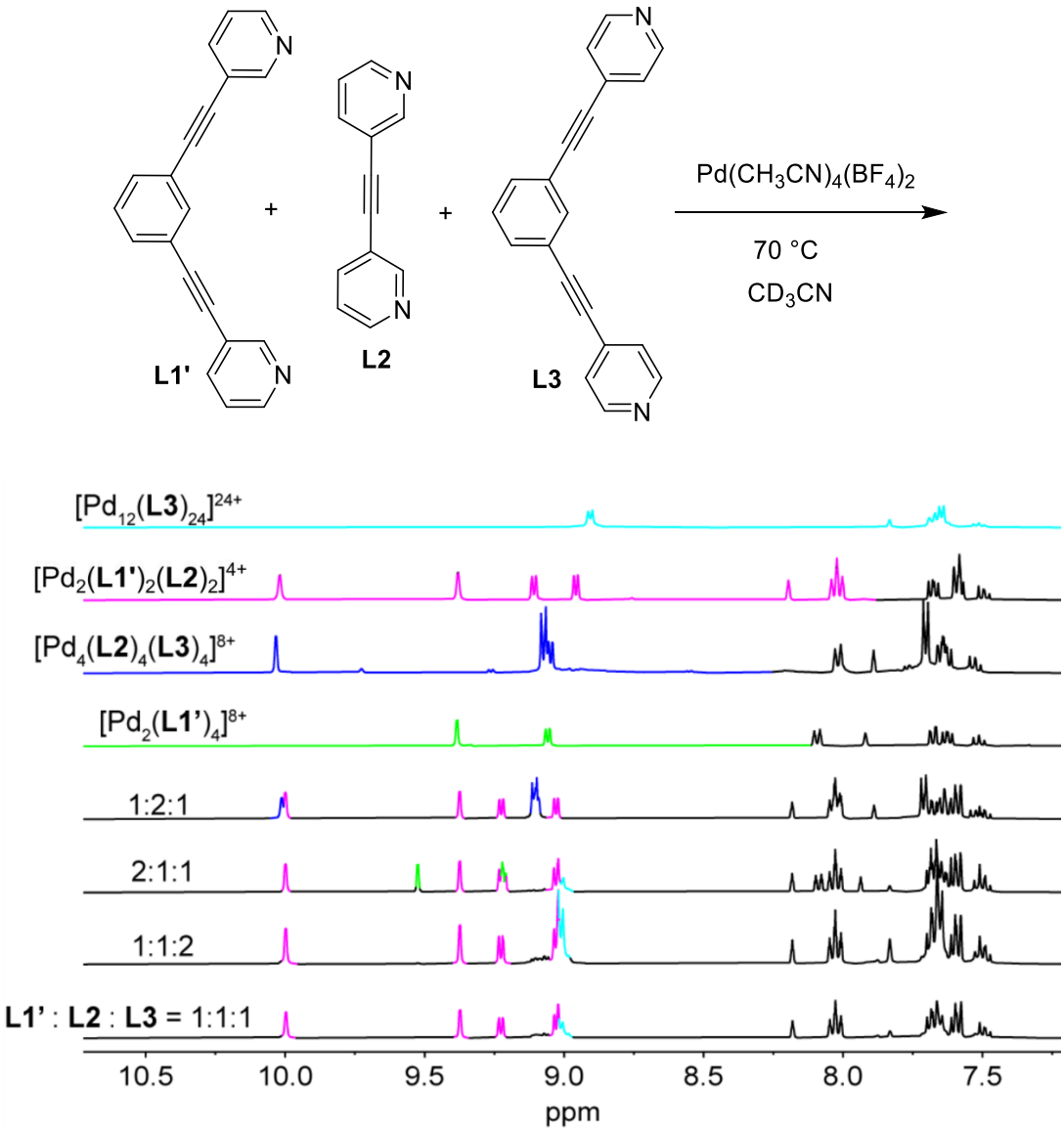

Figure S38. ^{1}H NMR spectra (400 MHz, CD_3CN) of equilibrated mixtures containing $[Pd(CH_3CN)_4](BF_4)_2$ and the ligands **L1'**, **L2**, and **L3** in different ratios ($[\mathbf{L}]_{total}$: [Pd] = 2:1). The spectra of $[Pd_{12}(\mathbf{L3})_{24}]^{24+}$, $[Pd_2(\mathbf{L1'})_2(\mathbf{L2})_2]^{4+}$, $[Pd_4(\mathbf{L2})_4(\mathbf{L3})_4]^{8+}$ and $[Pd_2(\mathbf{L1'})_4]^{4+}$ are given for comparison. Small changes in chemical shifts are likely due to intermolecular ligand-ligand interactions..

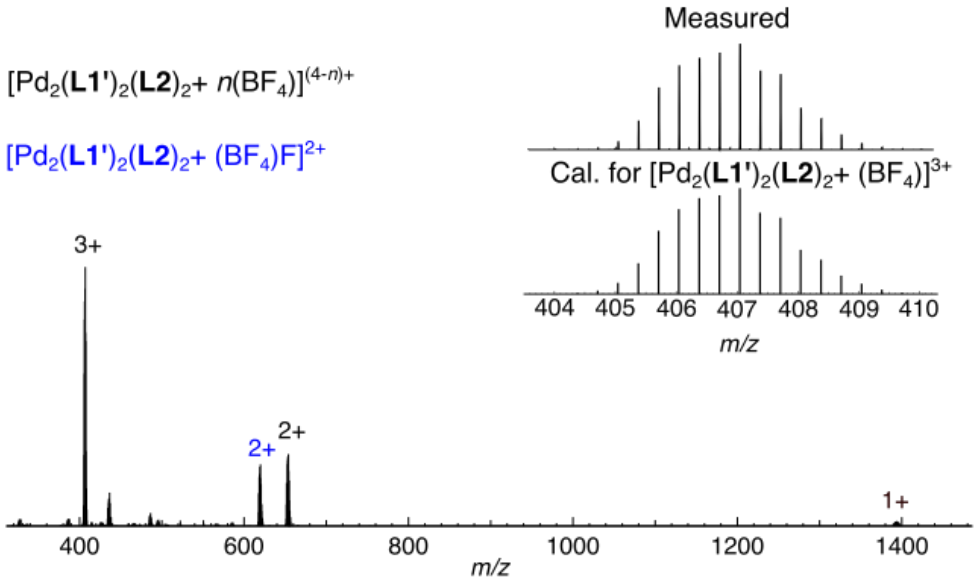

Figure S39. High-resolution ESI mass spectrum of an equilibrated mixture containing $[Pd(CH_3CN)_4](BF_4)_2$ and the ligands **L1'**, **L2**, and **L3** (1:1:1; $[\mathbf{L}]_{total}$: [Pd] = 2:1). Main peaks can be attributed to species of the formula $[Pd_2(\mathbf{L1'})_2(\mathbf{L2})_2 + n(BF_4)]^{(4-n)+}$.

4.3 Combination of **L1**, **L2'** and **L3**

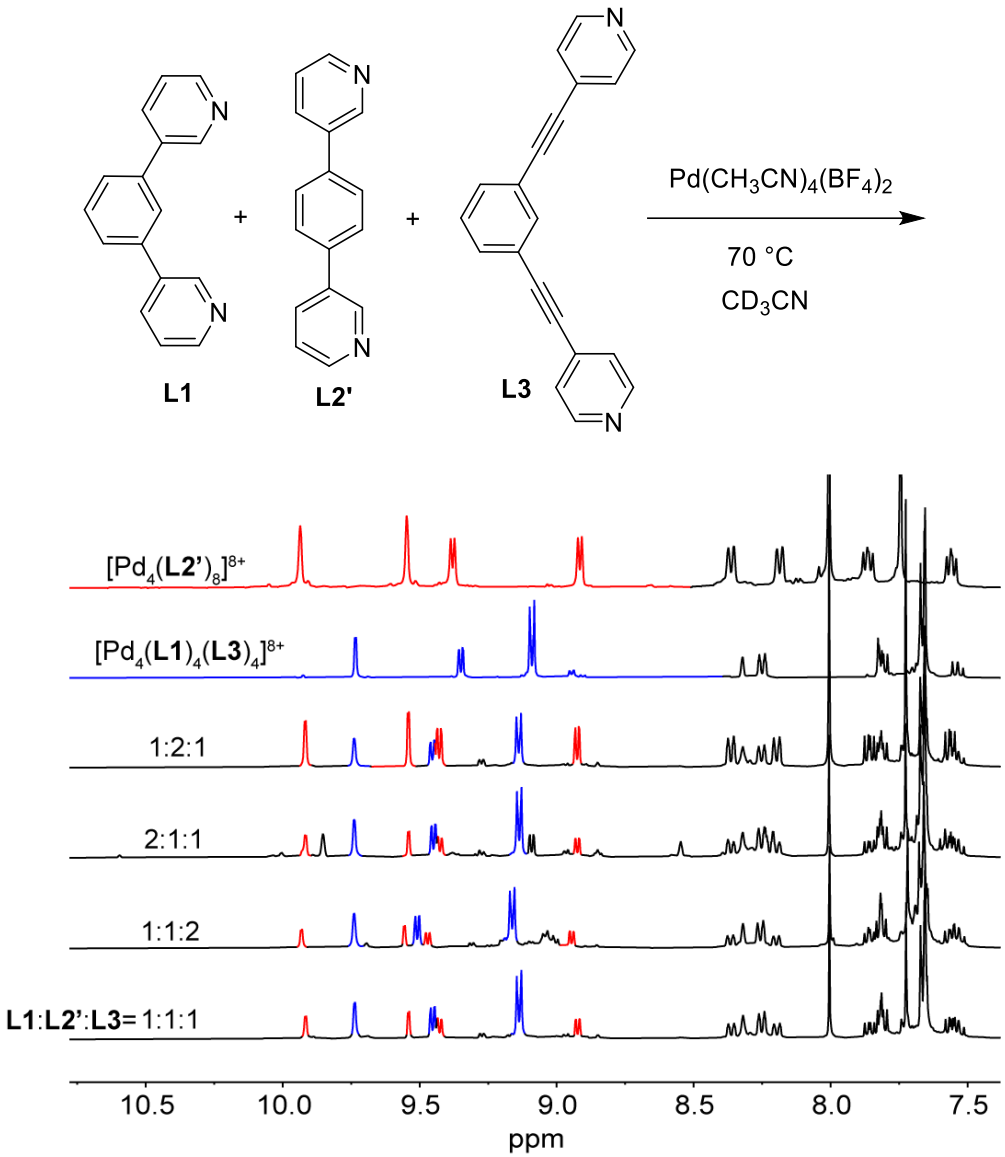

Figure S40. ^{1}H NMR spectra (400 MHz, CD_3CN) of equilibrated mixtures containing $[Pd(CH_3CN)_4](BF_4)_2$ and the ligands **L1**, **L2'**, and **L3** in different ratios ($[\mathbf{L}]_{total}$: [Pd] = 2:1). The spectra of $[Pd_4(\mathbf{L2'})_8]^{8+}$ and $[Pd_4(\mathbf{L1})_4(\mathbf{L3})_4]^{8+}$ are given for comparison.

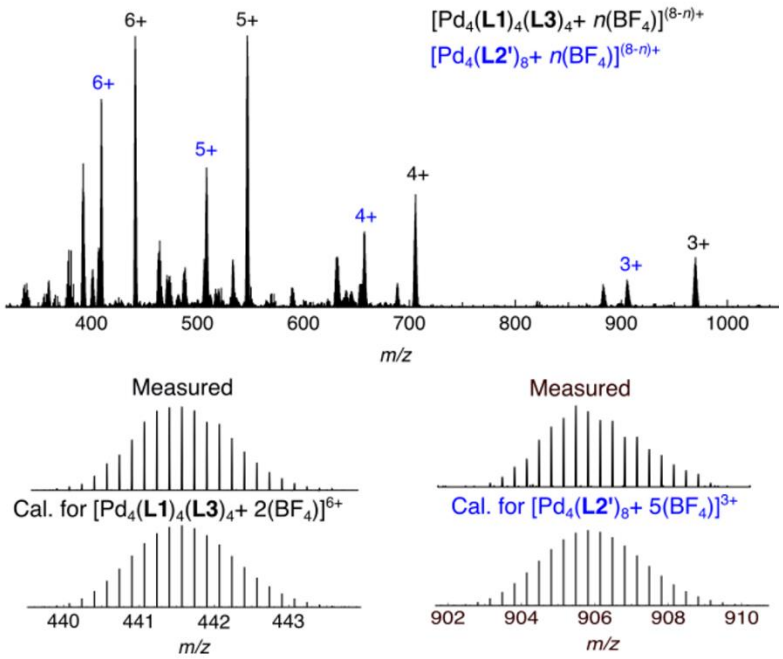

Figure S41. High-resolution ESI mass spectrum of an equilibrated mixture containing $[Pd(CH_3CN)_4](BF_4)_2$ and the ligands **L1**, **L2'**, and **L3** (1:1:1; $[\mathbf{L}]_{total}$: [Pd] = 2:1). Main peaks can be attributed to species of the formula $[Pd_4(\mathbf{L1})_4(\mathbf{L3})_4 + n(BF_4)]^{(8-n)+}$ and $[Pd_4(\mathbf{L2'})_8 + n(BF_4)]^{(8-n)+}$.

4.4 Combination of **L1**, **L2** and **L3'**

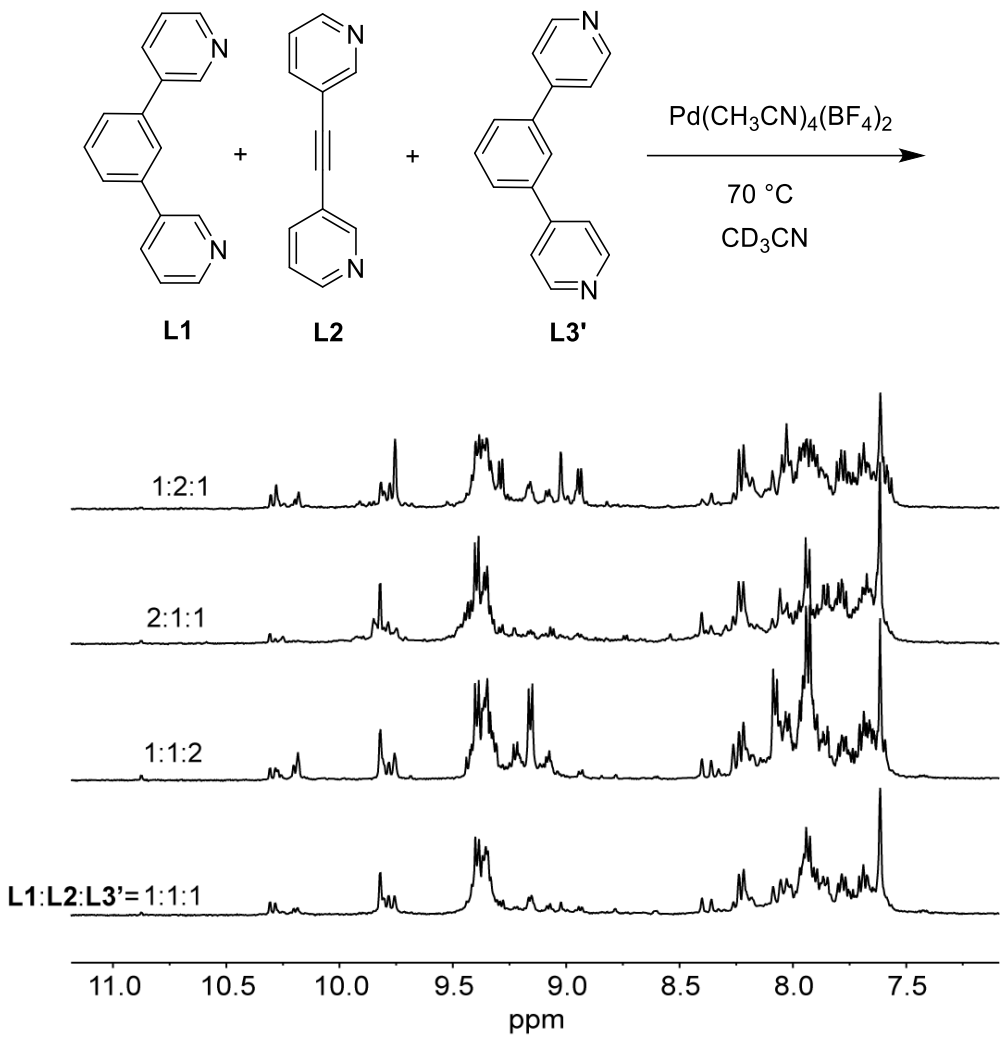

Figure S42. ^{1}H NMR spectra (400 MHz, CD_3CN) of equilibrated mixtures containing $[Pd(CH_3CN)_4](BF_4)_2$ and the ligands **L1**, **L2**, and **L3'** in different ratios ($[\mathbf{L}]_{total}$: [Pd] = 2:1).

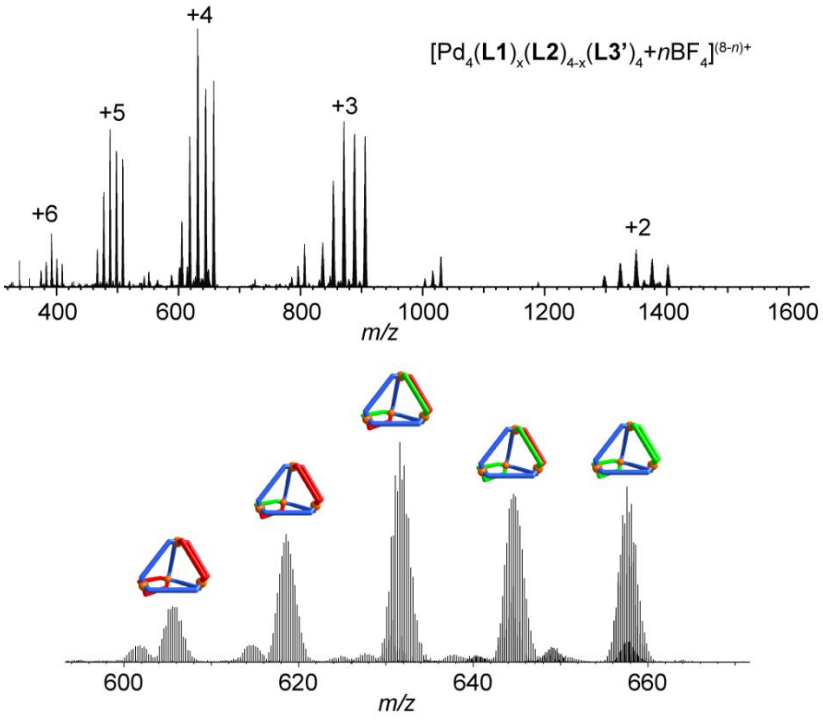

Figure S43. High-resolution ESI mass spectrum of an equilibrated mixture containing $[Pd(CH_3CN)_4](BF_4)_2$ and the ligands **L1**, **L2**, and **L3'** (1:1:2; $[\mathbf{L}]_{total}$: [Pd] = 2:1). Main peaks can be attributed to species of the formula $[Pd_4(\mathbf{L1})_x(\mathbf{L2})_{4-x}(\mathbf{L3'})_4+n BF_4]^{(8-n)+}$ (n = 2 – 6, x = 0 – 4).

4.5 Combination of **L1**, **L2'** and **L3'**

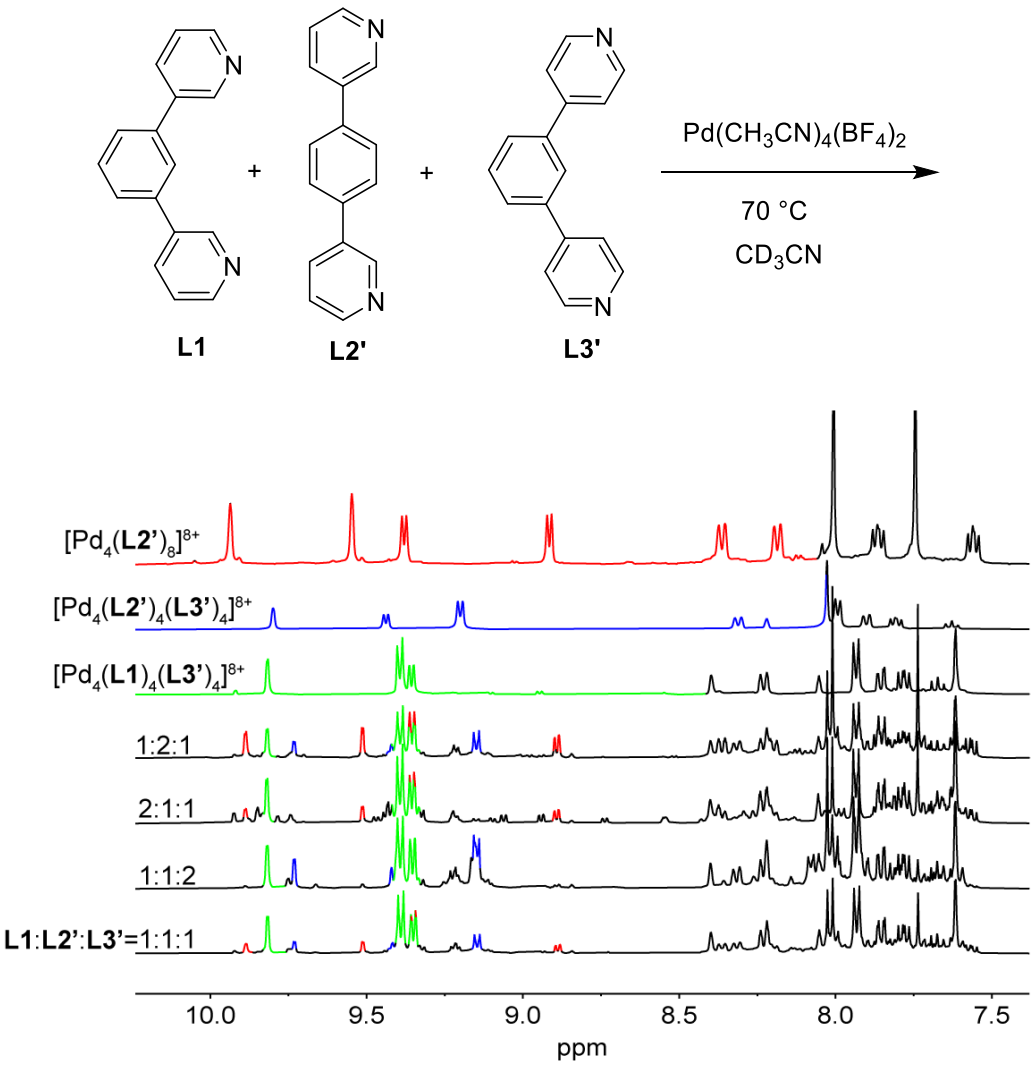

Figure S44. ^{1}H NMR spectra (400 MHz, CD_3CN) of equilibrated mixtures containing $[Pd(CH_3CN)_4](BF_4)_2$ and the ligands **L1**, **L2'**, and **L3'** in different ratios ($[\mathbf{L}]_{total}$: [Pd] = 2:1). The spectra of $[Pd_4(\mathbf{L2'})_8]^{8+}$, $[Pd_4(\mathbf{L2'})_4(\mathbf{L3})_4]^{8+}$, and $[Pd_4(\mathbf{L1})_4(\mathbf{L3'})_4]^{8+}$ are given for comparison. Small changes in chemical shifts are likely due to intermolecular ligand-ligand interactions..

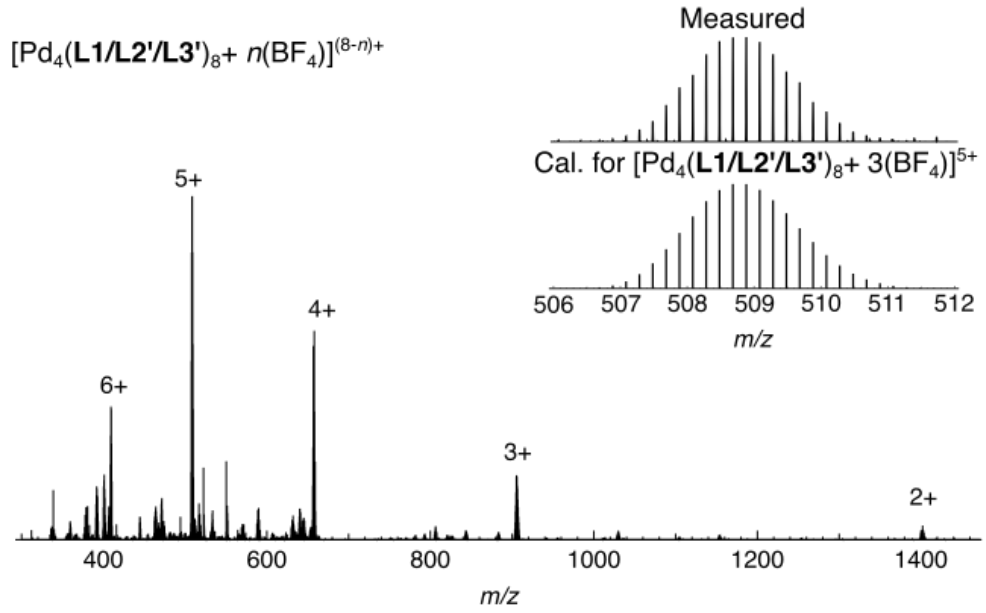

Figure S45. High-resolution ESI mass spectrum of an equilibrated mixture containing $[Pd(CH_3CN)_4](BF_4)_2$ and the ligands **L1**, **L2'**, and **L3'** (1:1:1; $[\mathbf{L}]_{total}$: [Pd] = 2:1). Main peaks can be attributed to species of the formula $[Pd_4(\mathbf{L1/L2'/L3'})_8 + n(BF_4)]^{(8-n)+}$.

4.6 Combination of **L1'**, **L2** and **L3'**

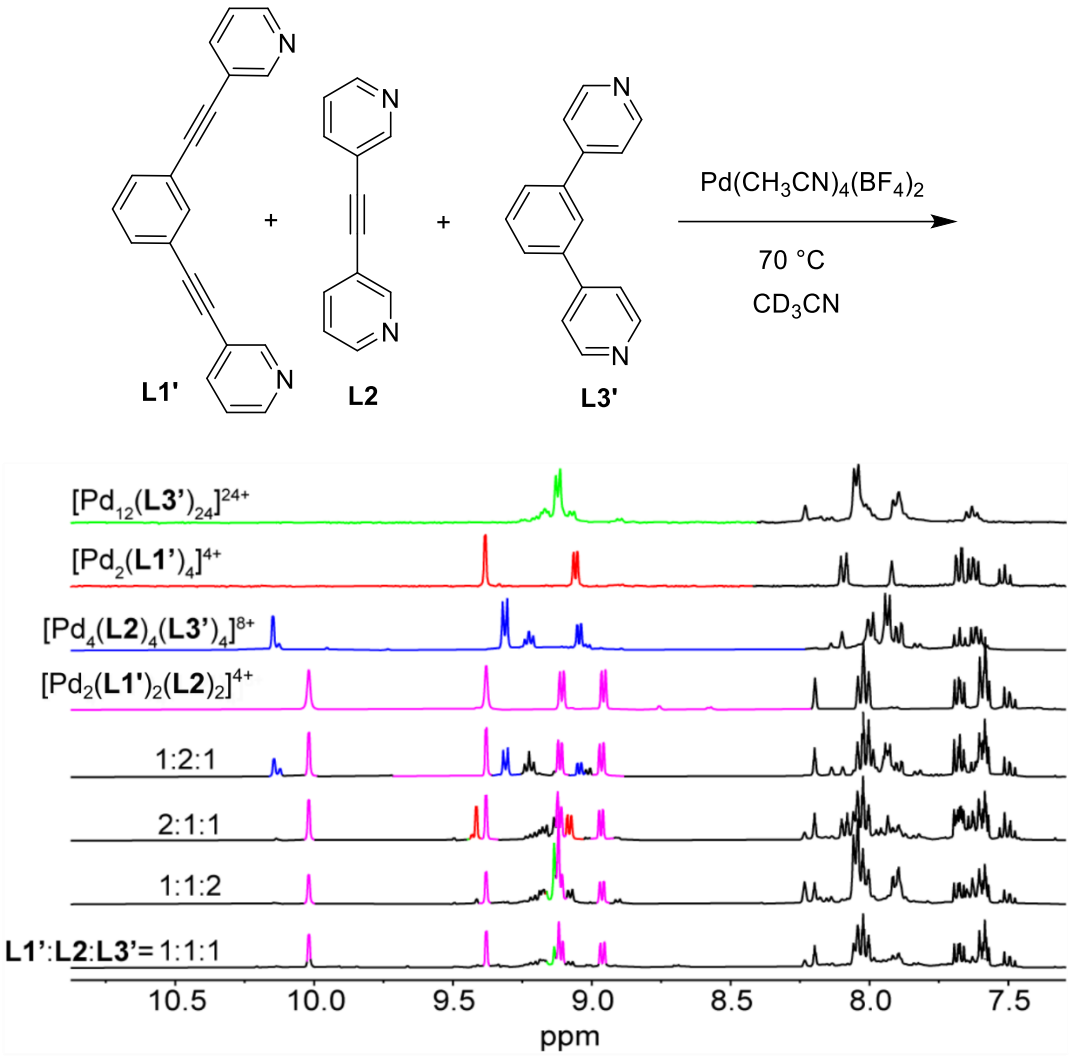

Figure S46. ^{1}H NMR spectra (400 MHz, CD_3CN) of equilibrated mixtures containing $[Pd(CH_3CN)_4](BF_4)_2$ and the ligands **L1'**, **L2**, and **L3'** in different ratios ($[\mathbf{L}]_{total}$: [Pd] = 2:1). The spectra of $[Pd_{12}(\mathbf{L3'})_{24}]^{24+}$, $[Pd_2(\mathbf{L1'})_4]^{4+}$, $[Pd_4(\mathbf{L2})_4(\mathbf{L3'})_4]^{8+}$ and $[Pd_2(\mathbf{L1'})_2(\mathbf{L2})_2]^{4+}$ are given for comparison.

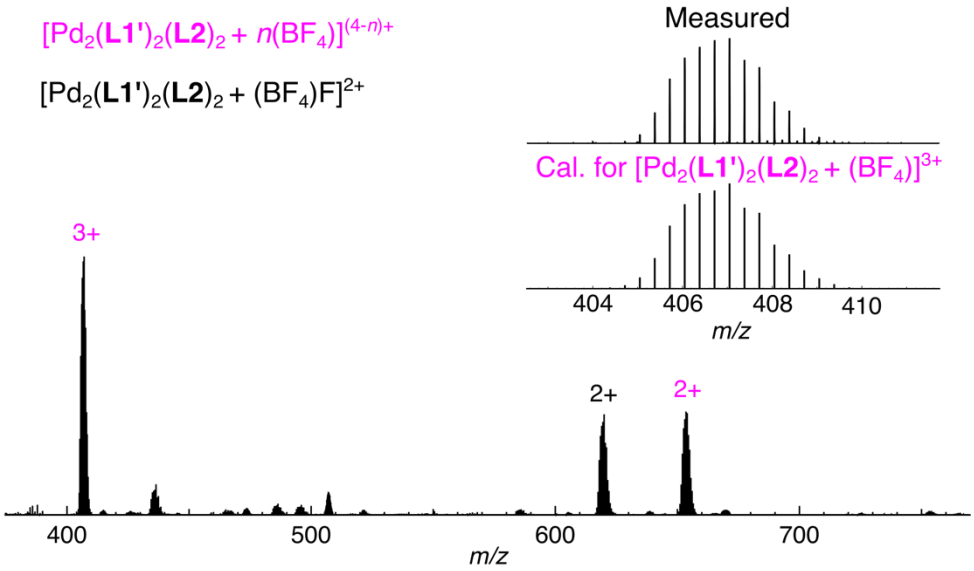

Figure S47. High-resolution ESI mass spectrum of an equilibrated mixture containing $[Pd(CH_3CN)_4](BF_4)_2$ and the ligands **L1'**, **L2**, and **L3'** (1:1:1; $[\mathbf{L}]_{total}$: [Pd] = 2:1). Main peaks can be attributed to species of the formula $[Pd_2(\mathbf{L1})_2(\mathbf{L2'})_2 + n(BF_4)]^{(4-n)+}$.

4.7 Combination of **L1'**, **L2'** and **L3**

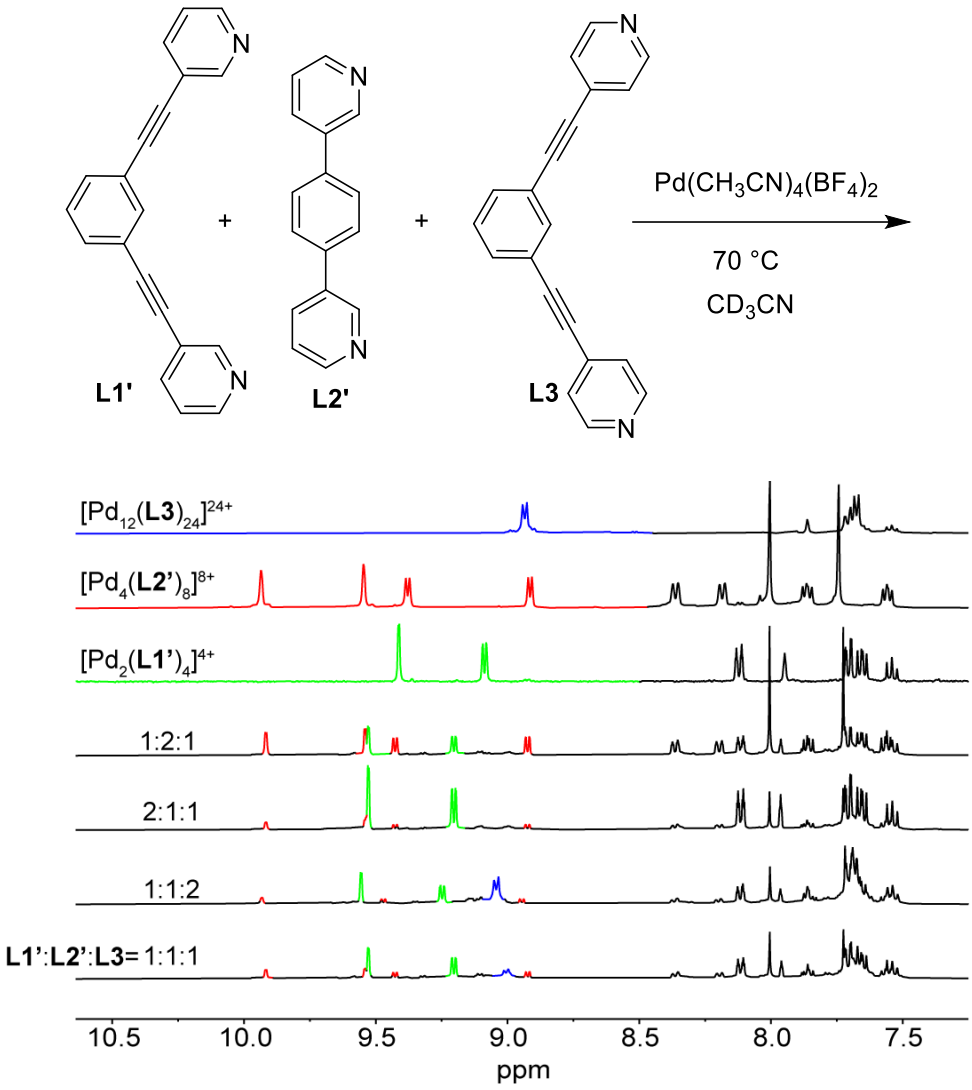

Figure S48. ^{1}H NMR spectra (400 MHz, CD_3CN) of equilibrated mixtures containing $[Pd(CH_3CN)_4](BF_4)_2$ and the ligands **L1'**, **L2'**, and **L3** in different ratios ($[\mathbf{L}]_{total}$: [Pd] = 2:1). The spectra of $[Pd_{12}(\mathbf{L3})_{24}]^{24+}$, $[Pd_4(\mathbf{L2'})_8]^{8+}$, and $[Pd_2(\mathbf{L1'})_4]^{4+}$ are given for comparison. Small changes in chemical shifts are likely due to intermolecular ligand-ligand interactions..

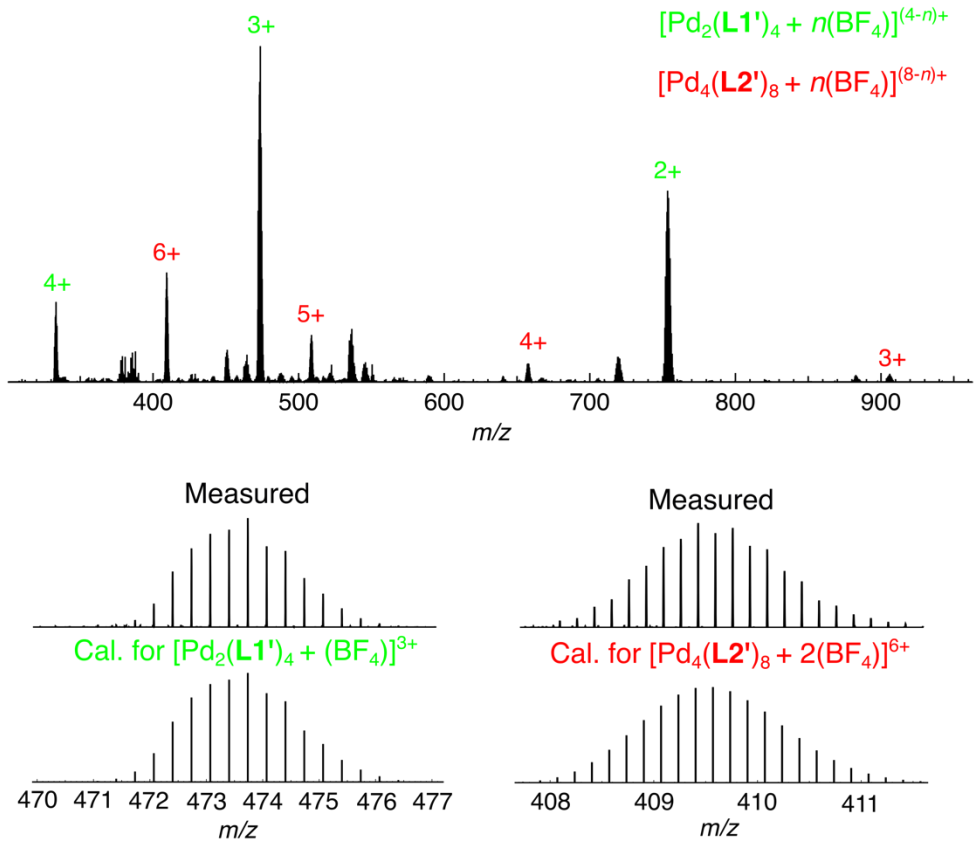

Figure S49. High-resolution ESI mass spectrum of an equilibrated mixture containing $[Pd(CH_3CN)_4](BF_4)_2$ and the ligands **L1'**, **L2'**, and **L3** (1:1:1; $[\mathbf{L}]_{total}$: [Pd] = 2:1). Main peaks can be attributed to species of the formula $[Pd_2(\mathbf{L1'})_4 + n(BF_4)]^{(4-n)+}$ and $[Pd_4(\mathbf{L2'})_8 + n(BF_4)]^{(8-n)+}$.

4.8 Combination of **L1'**, **L2'** and **L3'**

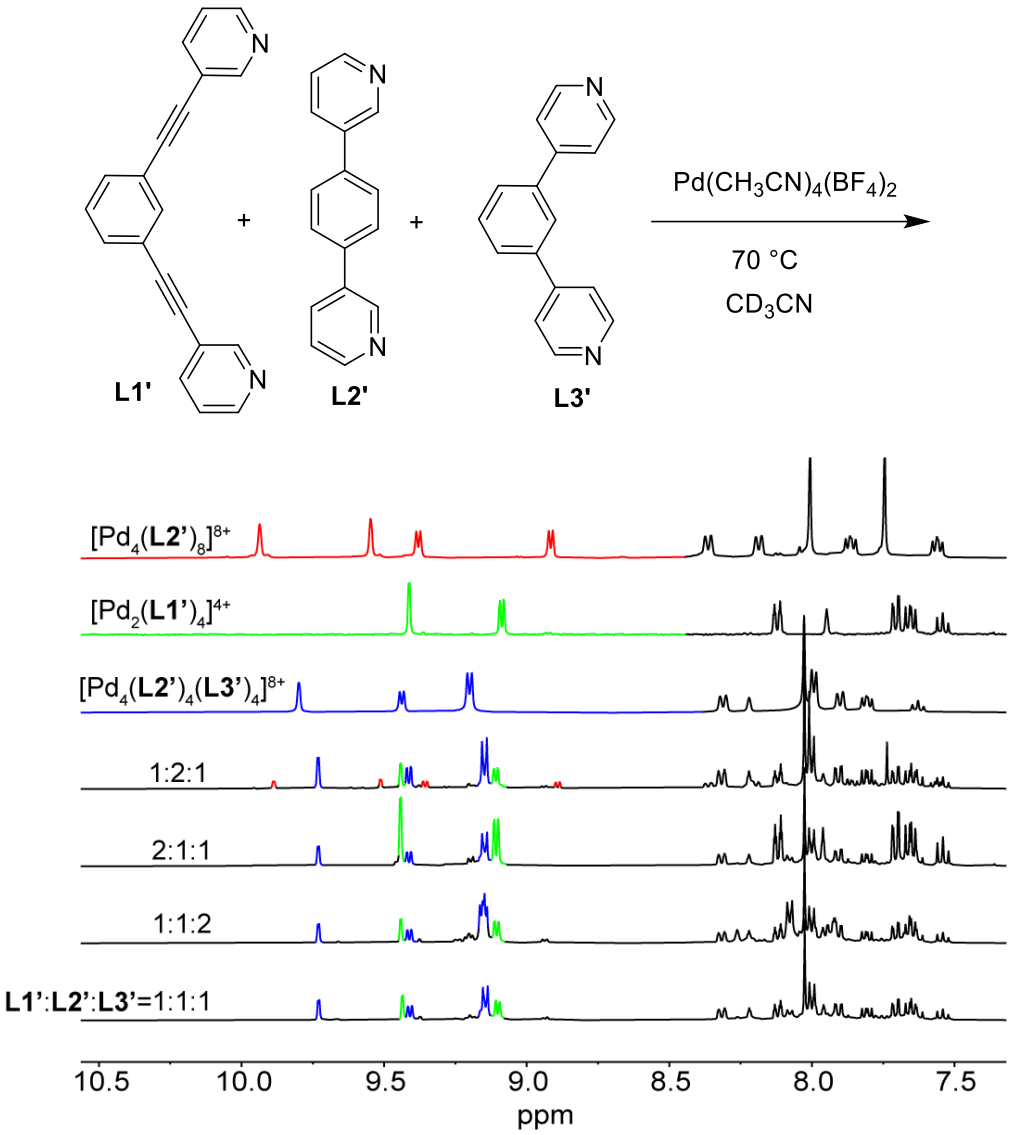

Figure S50. ^{1}H NMR spectra (400 MHz, CD_3CN) of equilibrated mixtures containing $[Pd(CH_3CN)_4](BF_4)_2$ and the ligands **L1'**, **L2'**, and **L3'** in different ratios ($[\mathbf{L}]_{total}$: [Pd] = 2:1). The spectra of $[Pd_4(\mathbf{L2'})_8]^{8+}$, $[Pd_2(\mathbf{L1'})_4]^{4+}$, and $[Pd_4(\mathbf{L2'})_4(\mathbf{L3'})_4]^{8+}$ are given for comparison. Small changes in chemical shifts are likely due to intermolecular ligand-ligand interactions.

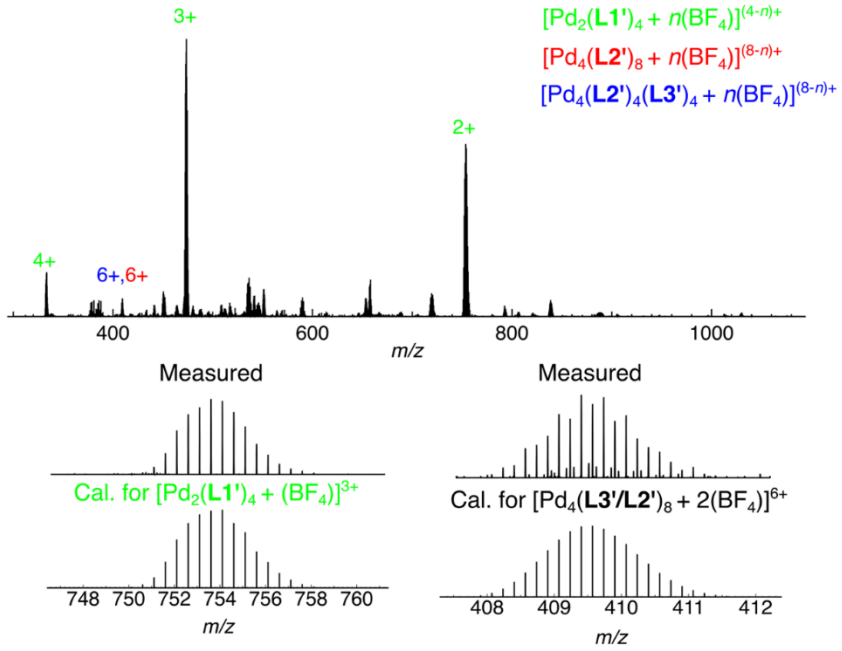

Figure S51 High-resolution ESI mass spectrum of an equilibrated mixture containing $[Pd(CH_3CN)_4](BF_4)_2$ and the ligands **L1'**, **L2'**, and **L3'** (1:1:1; $[L]_{total}$: [Pd] = 2:1). Main peaks can be attributed to species of the formula $[Pd_2(\mathbf{L1'})_4 + n(BF_4)]^{(4-n)+}$, $[Pd_4(\mathbf{L2'})_8 + n(BF_4)]^{(8-n)+}$ and $[Pd_4(\mathbf{L2'})_4(\mathbf{L3'})_4 + n(BF_4)]^{(8-n)+}$.

5. Crystallographic analyses

Single crystals of $[Pd_4(\mathbf{L2})_8](BF_4)_8$ were obtained by slow (several weeks) vapor diffusion of diisopropyl ether into a CH_3CN solution of $[Pd_4(\mathbf{L2})_8](BF_4)_8$ (1.13 mM). Single crystals of $[Pd_4(\mathbf{L2})_4(\mathbf{L3})_4](BF_4)_8$ were obtained by slow (several weeks) vapor diffusion of diisopropyl ether into a CH_3CN solution of $[Pd_4(\mathbf{L2})_4(\mathbf{L3})_4](BF_4)_8$ (1.13 mM). Single crystals of $[Pd_4(\mathbf{L1})_2(\mathbf{L2})_2(\mathbf{L3})_4](BF_4)_8$ were obtained by slow (several weeks) vapor diffusion of diethyl ether into a CH_3CN solution containing a mixture of $[Pd_4(\mathbf{L1})_x(\mathbf{L2})_{4-x}(\mathbf{L3})_4](BF_4)_8$ complexes for several weeks. Crystals of $[Pd_2(\mathbf{L1'})_2(\mathbf{L2})_2](BF_4)_4$ were obtained by slow (several weeks) vapor diffusion of diethyl ether into a CH_3CN solution of $[Pd_2(\mathbf{L1'})_2(\mathbf{L2})_2](BF_4)_4$ (2.25 mM).

Details for the analysis of $[Pd_4(L2)_8](BF_4)_8$:

A colourless prism-shaped crystal with dimensions of 0.50 × 0.34 × 0.13 mm^3 was mounted. Data were collected using a SuperNova, Dual, Cu at home/near, Atlas diffractometer operating at T = 140.00(10) K.

Data were measured using ω scans using Mo$K\alpha$ radiation. The diffraction pattern was indexed and the total number of runs and images was based on the strategy calculation from the program CrysAlis^{Pro}.[S8] The maximum resolution achieved was Θ = 26.372° (0.80 Å).

The diffraction pattern was indexed and the total number of runs and images was based on the strategy calculation from the program CrysAlis^{Pro}. The unit cell was refined using CrysAlis^{Pro} on 7365 reflections, 32% of the observed reflections.

Data reduction, scaling and absorption corrections were performed using CrysAlis^{Pro}. The final completeness is 99.60% out to 26.372° in Θ. A Gaussian absorption correction was performed using CrysAlisPro. Numerical absorption correction based on Gaussian integration over a multifaceted crystal model. Empirical absorption correction using spherical harmonics as implemented in SCALE3 ABSPACK scaling algorithm. The absorption coefficient μ of this material is 0.434 mm^{-1} at this wavelength (λ = 0.71073Å) and the minimum and maximum transmissions are 0.475 and 1.000.

The structure was solved in the space group $C2$ (# 5) by the ShelXT[S9] structure solution program using dual methods and refined by full-matrix least-squares minimisation on $\boldsymbol{F^2}$ using ShelXL.[S10] All non-hydrogen atoms were refined anisotropically. Hydrogen atom positions were calculated geometrically and refined using the riding model. The model was refined as a 2-component inversion twin.

The value of Z' is 0.5. This means that only half of the formula unit is present in the asymmetric unit, with the other half consisting of symmetry-equivalent atoms.

The Flack parameter was refined to 0.422(15). Determination of absolute structure using Bayesian statistics on Bijvoet differences using the Olex2[S11] results in None.

Note: Additional counter-ions and solvent molecules, too disordered to be located in the electron density map, were taken into account using the Olex2[S11] solvent-mask procedure.

Details for the analysis of $[Pd_4(L2)_4(L3)_4](BF_4)_8$:

A colorless prism-shaped crystal with dimensions of 0.36 × 0.26 × 0.08 mm^3 was mounted. Data were collected using a SuperNova, Dual, Cu at home/near, AtlasS2 diffractometer operating at T = 140.00(10) K.

Data were measured using ω scans with Cu K_α radiation. The diffraction pattern was indexed and the total number of runs and images was based on the strategy calculation from the program CrysAlis^{Pro}. The maximum resolution that was achieved was Θ = 50.432˚ (1.00 Å).

The unit cell was refined using CrysAlis^{Pro} on 4727 reflections, 9% of the observed reflections.

Data reduction, scaling and absorption corrections were performed using CrysAlis^{Pro}. The final completeness is 99.00% out to 50.432˚ in Θ. An analytical absorption correction was performed using CrysAlis^{Pro}. The analytical numeric absorption correction was done using a multifaceted crystal model based on expressions derived by R.C. Clark & J.S. Reid.[S12] The empirical absorption correction was obtained using spherical harmonics, implemented in SCALE3 ABSPACK scaling algorithm. The absorption coefficient μ of this crystal is 3.617 mm^{-1} at this wavelength (λ = 1.54184Å) and the minimum and maximum transmissions are 0.349 and 0.708.

The structure was solved and the space group $P2_1/n$ (# 14) determined by the ShelXT[S8] structure solution program using iterative methods and refined by full matrix least squares minimisation on $\boldsymbol{F^2}$ using ShelXL.[S9] All non-hydrogen atoms were refined anisotropically. Hydrogen atom positions were calculated geometrically and refined using the riding model.

_twin_special_details: Component 2 rotated by -172.7010˚ around [0.01 0.99 -0.14] (reciprocal) or [-0.00 1.00 -0.02] (direct)

Note: The crystal diffracted very badly and poorly, resulting in A and B level alerts in the CheckCif file. The obtained model needs several restraints and contraints to finally converge. The anions (8 BF_4^-) and the solvent molecules were not easily located on the difference map. In order to improve the model, a solvent mask algorithm based on BYPASS[S12] was employed to subtract the electron density in the solvent (and anion) area.

Details for the analysis of $[Pd_4(L1)_2(L2)_2(L3)_4](BF_4)_8$:

A colourless prism-shaped crystal with dimensions of 0.16 × 0.12 × 0.09 mm^3 was mounted. Data were collected using an XtaLAB Synergy R, DW system, HyPix-Arc 150 diffractometer operating at T = 140.00(10) K.

Data were measured using ω scans with Cu$K\alpha$ radiation. The diffraction pattern was indexed and the total number of runs and images was based on the strategy calculation from the program CrysAlis^{Pro}. The maximum resolution achieved was Θ = 39.973˚ (1.20 Å).

The unit cell was refined using CrysAlis^{Pro} on 30138 reflections, 42% of the observed reflections.

Data reduction, scaling and absorption corrections were performed using CrysAlis^{Pro}. The final completeness is 99.70 % out to 39.973˚ in Θ. A Gaussian absorption correction was performed using CrysAlis^{Pro}. Numerical absorption correction based on Gaussian integration over a multifaceted crystal model. Empirical absorption correction using spherical harmonics as implemented in SCALE3

ABSPACK scaling algorithm. The absorption coefficient μ of this material is 3.278 mm^{-1} at this wavelength (λ = 1.54184Å) and the minimum and maximum transmissions are 0.710 and 1.000.

The structure was solved in the space group $P\bar{1}$ (# 2) by the ShelXT structure solution program using dual methods and refined by full-matrix least-squares minimisation on F^2 using ShelX. All non-hydrogen atoms were refined anisotropically. Hydrogen atom positions were calculated geometrically and refined using the riding model. The data quality was low due to the extremely weak diffraction of this crystal. The RIGU and SIMU restraints were applied to all the atoms.

Note: Additional counter-ions and solvent molecules, too disordered to be located in the electron density map, were taken into account using the Olex2[S10] solvent-mask procedure.

Details for the analysis of $[Pd_2(L1')_2(L2)_2](BF_4)_4$:

A colourless prism-shaped crystal with dimensions of 0.21 × 0.12 × 0.07 mm^3 was mounted. Data were collected using an XtaLAB Synergy R, DW system, HyPix-Arc 150 diffractometer operating at T = 139.99(10) K.

Data were measured using ω scans with Cu$K\alpha$ radiation. The diffraction pattern was indexed and the total number of runs and images was based on the strategy calculation from the program CrysAlis[Pro]. The maximum resolution achieved was Θ = 74.693° (0.80 Å).

The unit cell was refined using CrysAlis[Pro] on 27685 reflections, 48% of the observed reflections.

Data reduction, scaling and absorption corrections were performed using CrysAlis[Pro]. The final completeness is 99.70 % out to 74.693° in Θ. A Gaussian absorption correction was performed using CrysAlis[Pro]. Numerical absorption correction based on Gaussian integration over a multifaceted crystal model. Empirical absorption correction using spherical harmonics as implemented in SCALE3 ABSPACK scaling algorithm. The absorption coefficient μ of this material is 4.460 mm^{-1} at this wavelength (λ = 1.54184Å) and the minimum and maximum transmissions are 0.623 and 0.898.

The structure was solved in the space group $P2_1$ (# 4) by the ShelXT structure solution program using using dual methods and refined by full-matrix least-squares minimisation on F^2 using ShelXL. All non-hydrogen atoms were refined anisotropically. Hydrogen atom positions were calculated geometrically and refined using the riding model.

The model was refined as a 2-component inversion twin.

A solvent mask was calculated and 556 electrons were found in a volume of 2126 $Å^3$ in three voids per unit cell. This is consistent with the presence of six molecules of acetonitrile per Asymmetric Unit which account for 528 electrons per unit cell.

The value of Z' is 2. This means that there are two independent molecules in the asymmetric unit.

The Flack parameter was refined to 0.245(9). Determination of absolute structure using Bayesian statistics on Bijvoet differences using the Olex2 results in None.

Crystallographic and refinement data of $[Pd_4(\mathbf{L2})_8](BF_4)_8$, $[Pd_4(\mathbf{L2})_4(\mathbf{L3})_4](BF_4)_8$, $[Pd_4(\mathbf{L1})_2(\mathbf{L2})_2(\mathbf{L3})_4](BF_4)_8$, and $[Pd_2(\mathbf{L1'})_2(\mathbf{L2})_2](BF_4)_4$ are summarized in Table S1 and Table S2.

Table S1. Crystal data and structure refinement for $[Pd_4(\mathbf{L2})_8](BF_4)_8$ and $[Pd_4(\mathbf{L2})_4(\mathbf{L3})_4](BF_4)_8$.

Compound	$[Pd_4(\mathbf{L2})_8](BF_4)_8$	$[Pd_4(\mathbf{L2})_4(\mathbf{L3})_4](BF_4)_8$
Formula	$C_{96}H_{64}N_{16}Pd_4$	$C_{128}H_{80}N_{16}Pd_4$
$D_{calc.}$/ g cm^{-3}	0.713	0.878
μ/mm^{-1}	0.434	3.617
Formula Weight	1867.23	2267.68
Color	colorless	colorless
Shape	prism	prism-shaped
Size/mm^3	0.50×0.34×0.13	0.36×0.26×0.08
T/K	140.00(10)	140.00(10)
Crystal System	monoclinic	monoclinic
Space Group	$C2$	$P2_1/n$
a/Å	28.1944(18)	25.5096(19)
b/Å	18.4331(18)	16.3107(10)
c/Å	17.3971(12)	41.832(3)
α/°	90	90
β/°	105.824(7)	99.765(6)
γ/°	90	90
V/Å^3	8698.8(12)	17153(2)
Z	2	4
Z'	0.5	1
Wavelength/Å	0.71073	1.54184
Radiation type	Mo$K\alpha$	Cu$K\alpha$
Θ_{min}/°	3.038	2.914
Θ_{max}/°	26.372	50.432
Measured Refl's.	23318	54539
Ind't Refl's	14777	17792
Refl's with I > 2σ(I)	9177	6785
R_{int}	0.0354	0.1072
Parameters	428	1093
Restraints	880	1698
Largest Peak/e Å^{-3}	0.232	0.696
Deepest Hole/e Å^{-3}	–0.156	–0.636
GooF	0.823	0.936
wR_2 (all data)	0.0777	0.3568
wR_2	0.0683	0.3319
R_1 (all data)	0.0605	0.1757
R_1	0.0335	0.1176
CCDC number	2237747	2236122

Table S2. Crystal data and structure refinement for $[Pd_4(\mathbf{L1})_2(\mathbf{L2})_2(\mathbf{L3})_4](BF_4)_8$ and $[Pd_2(\mathbf{L1'})_2(\mathbf{L2})_2](BF_4)_4$.

Compound	$[Pd_4(\mathbf{L1})_2(\mathbf{L2})_2(\mathbf{L3})_4](BF_4)_8$	$[Pd_2(\mathbf{L1'})_2(\mathbf{L2})_2](BF_4)_4$
Formula	$C_{136}H_{88}N_{16}Pd_4$	$C_{64}H_{40}B_4F_{16}N_8Pd_2$
$D_{calc.}$/ g cm^{-3}	0.828	1.280
μ/mm^{-1}	3.278	4.460
Formula Weight	2371.82	1481.08
Color	colourless	colourless
Shape	prism-shaped	prism-shaped
Size/mm^3	0.16×0.12×0.09	0.21×0.12×0.07
T/K	140.00(10)	139.99(10)
Crystal System	triclinic	monoclinic
Space Group	$P\bar{1}$	$P2_1$
a/Å	19.4282(7)	11.3697(2)
b/Å	21.0392(5)	65.3984(8)
c/Å	24.7683(6)	11.7619(2)
α/°	91.918(2)	90
β/°	109.850(3)	118.507(3)
γ/°	91.610(2)	90
V/Å^3	9508.8(5)	7685.3(3)
Z	2	4
Z'	1	2
Wavelength/Å	1.54184	1.54184
Radiation type	Cu$K\alpha$	Cu$K\alpha$
Θ_{min}/°	2.420	2.703
Θ_{max}/°	39.973	74.693
Measured Refl's.	70982	57817
Ind't Refl's	11503	26588
Refl's with I > 2σ(I)	7922	22790
R_{int}	0.0789	0.0361
Parameters	1153	1693
Restraints	2382	2729
Largest Peak/e Å^{-3}	0.913	0.974
Deepest Hole/e Å^{-3}	–0.858	-1.027
GooF	1.671	1.121
wR_2 (all data)	0.4032	0.1748
wR_2	0.3805	0.1698
R_1 (all data)	0.1428	0.0703
R_1	0.1177	0.0620
CCDC number	2236714	2237144

6. References

S1 B. Avitia, E. MacIntosh, S. Muhia and E. Kelson, *Tetrahedron Lett*., 2011, **52**, 1631–1634.

S2 P. Liao, B. W. Langloss, A. M. Johnson, E. R. Knudsen, F. S. Tham, R. R. Julian and R. J. Hooley, *Chem. Commun*. 2010, **46**, 4932–4934.

S3 E. Bosch and C. L. Barnes, *New J. Chem.*, 2001, **25**, 1376–1378.

S4 M. Schulze, V. Kunz, P. D. Frischmann and F. Würthner, *Nat. Chem*., 2016, **8**, 576–583.

S5 T. Kikuchi,T. Murase, S. Sato and M. Fujita, *Supramol. Chem*., 2008, **20**, 81–94.

S6 L. Zeng, Y. Xiao, J. Jiang, H. Fang, Z. Ke, L. Chen and J. Zhang, *Inorg. Chem*., 2019, **58**, 10019−10027.

S7 S. Sudan, R. Li, S. Jansze, A. Platzek, R. Rudolf, G. H. Clever, F. Fadaei Tirani, R. Scopelliti and K. Severin, *J. Am. Chem. Soc.*, 2021, **143**, 1773–1778

S8 *CrysAlis*^{Pro} software system, Rigaku Oxford Diffraction.

S9 G. M. Sheldrick, *Acta Cryst.*, 2015, **A71**, 3–8.

S10 G. M. Sheldrick, *Acta Cryst.*, 2015, **C71**, 3–8.

S11 O. V. Dolomanov, J. L. Bourhis, R. J. Gildea, J. A. K. Howard and H. Puschmann, *J. Appl. Cryst.*, 2009, **42**, 339–341.

S12 R. C. Clark and J. S. Reid, *Acta Cryst*., 1995, **A51**, 887–897.

S13 P. van der Sluis and A. L. Spek, *Acta Cryst.*, 1990, **A46**, 194–201.